

FINAL REPORT

Project Funded through



Developing Enhanced Marine Operations (DEMO) in High Flow Tidal Environments

Industry Partners

Dynamic Systems Analysis Ltd. / AML Oceanographic

By

NSCC Applied Research, Engineered Technologies Lab

Ivany Campus, Dartmouth NS

Contacts:

Dr. Etienne Mfoumou, *Research Scientist*, etienne.mfoumou@nsc.ca, Tel: 902-491-1692

Ms. Beth McCormack, *Community Innovation Lead*, beth.mccormack@nsc.ca, Tel: 902-491-7340

This report was prepared by:

NSCC Applied Research,
Engineered Technologies Lab,
Nova Scotia Community College
80 Mawiomi Place,
Dartmouth, Nova Scotia
B2Y 0A8

The project was funded under the:
Offshore Energy Research Association (OERA)

November 28, 2019

TABLE OF CONTENTS

Table of Contents

Table of Contents	3
Summary	Error! Bookmark not defined.
I- INTRODUCTION AND OBJECTIVES	6
II- TARGET SITE LOCATION FOR FIELD TESTING	7
III- EXPECTED MILESTONES	7
III-1- Work Package 1 (Phase #1):	7
III-2- Work Package 2 (Phase #2):	7
III-3- Work Package 3 (Phase #3):	8
III-4- Work Package 4 (Phase #4):	8
III-5- Important update	10
IV- ROV AND UMBILICAL MODELING	10
IV-1- Reference frames.....	10
IV-2- Umbilical governing equations	11
IV-3- Umbilical boundary conditions.....	11
IV-4 Umbilical external loads.....	13
IV-5- ROV governing equation	13
V- COMPUTER-AIDED DESIGN (CAD) MODELING, MESHING AND SIMULATION .	13
V-1- CAD modeling and meshing	13
V-2- Simulation data generation.....	15
Work Package 1	15
Work Package 2	24
VI- PLANNING EXPERIMENTAL VALIDATION OF SIMULATED RESULTS	30
VI-1- Approach used.....	30
VI-2- Proposed activities for tank testing	33

VII-	MODELING CAPABILITIES IMPROVEMENT EFFORTS.....	43
VII-1-	Estimating hydrodynamic parameters of the ROV.....	43
	Scope.....	43
	Numerical configuration and simulation	44
	ShipMo3D simulation results	46
VII-2-	Simulation-based optimization	49
VIII-	EXPERIMENTAL VALIDATION OF SIMULATED RESULTS.....	51
VIII-1-	The Aquatron pool tank.....	51
VIII-2-	Description and features of the Falcon ROV	52
VIII-3-	Experimental Procedure	55
VIII-4-	Data processing	56
VIII-5-	Results and interpretation.....	56
	ROV only (no skid).....	56
	ROV with Skid.....	60
IX-	CONCLUSIONS.....	60
X-	RECOMMENDATIONS.....	61
XI-	BUDGET	62
XII-	EMPLOYMENT SUMMARY	62

SUMMARY

ROV use in new and emerging areas including marine renewable energy and seafloor characterization in high flow environment is growing. With the downturn in the oil and gas industry, there is a reduced level of activity in the marine ROV operations related to the industry. Cost reduction and improved capabilities have become the priorities for ROV development. In this context, the current state of research in the use of a ROV in high flow marine environments is still limited, and none have been conducted in the Bay of Fundy. While the development and technical advances in the capability of ROVs has expanded their utility in underwater operations, these vehicles range in size from very small ‘observation’ role systems weighing a few kilograms, to very large class III and IV ROVs weighing many tons, designed for complex underwater engineering tasks. The opportunities afforded using ROVs to maximize efficiency and increase the effectiveness of marine operations in high flow tidal environment, clearly makes practical and financial sense.

This Project consists of the work and deliverables described in the Recipient’s proposal entitled: *Developing Enhanced Marine Operations (DEMO) in High Flow Tidal Environments* dated August 8, 2017. The project was defined as three work packages. The first one has established baseline capabilities of a selected ROV to be tested in the Bay of Fundy. The research team has successfully conducted a technical pre-assessment of the Cougar XT-1420 ROV capabilities through computer simulation of ROV thrusters’ performance analysis. To generate the results, a 3D CAD model as well as a mesh of the ROV were developed. These capabilities were established with consideration of the current marine renewable sites in the Digby and Minas Passage areas. NSCC has assessed the technical feasibility of deploying an ROV in selected sites, based on Dominion Diving’s marine assets and expertise to conduct testing in the Bay of Fundy and to develop the technology upgrade required to successfully complete the DEMO research program.

Work Package 2 has contributed to the development of modeling capabilities that apply the outcome of the previous phase toward developing a set of tools that will help reduce the risks associated with operations in high flow tidal environments. The capabilities being developed can also be used to assess optimization requirements to existing marine assets. This has built on expertise developed by the Heuristic and Evolutionary Algorithms Laboratory of the School of Informatics, Communications and Media of the University of Applied Sciences in Upper Austria (NSCC’s partner). Dynamic Systems Analysis Ltd. (DSA) has provided dynamic analysis software and expertise to assess the motions and loads on the proposed ROV configurations, to reduce operation risks in planning a deployment in high flow tidal environments. The results suggested conducting validation tests in a controlled environment, which was done as part of Work Package 3 in the Aquatron facility at Dalhousie University. A better understanding of the deployment limits was gained as the forward relative fluid velocity increased, and this was used to improve existing modeling capabilities.

I- INTRODUCTION AND OBJECTIVES

The high-energy Bay of Fundy marine environment offers a vast relatively untapped source of renewable energy in the form of tides. In this context, energy conversion technologies that harvest this energy source are increasingly coming on-line, and dependable tools that can be used to inspect and interact with submerged infrastructure over sustained periods are increasingly needed. In the past few years, the Nova Scotia tidal community has augmented its marine operational capacity, but some unknowns and risks still exist, and the cost associated with such operations are high. A next step in reducing tidal energy levelized costs is therefore improving the performance of key installation tools, such as Remotely Operated Vehicles (ROVs).

The proposed original DEMO project intended to enhance marine operations capacity and efficiencies in the Bay of Fundy high flow tidal environments. This was required for cost reduction (e.g. minimize diver involvement or frequency of inspection), operational safety (e.g. minimize diver or rope access technician involvement), and the overall advancement of marine renewable energy industry in Canada. The project also expected to provide additional value to the marine renewable infrastructure available to service this industry as it moves towards commercialization.

The cancellation of the Bay of Fundy field trials due to lack of (cash/in-kind) leverage funding has led to a scope revision. The revised scope is focused on completing modeling and design characteristics for the Cougar ROV, that will lead to improvements in ROV operations and efficiency suitable to high flow marine environments. Consideration was given to the work being done with DSA such as hydrodynamic coefficients, thrusters performance, and incorporating the results of testing conducted in a controlled environment, to improve existing modeling capabilities. This will help to achieve Nova Scotia's vision to be a global leader in the development of technology and systems that produce environmentally sustainable and competitively priced electricity from the ocean. However, the project does not only deliver innovation in the marine renewable energy sector early-stage supply chain but also provides tools to address the challenges faced by decision makers and companies operating in the sector. Moreover, the pace of technology development requires that students have exposure to state-of-the-art facilities and access to leading-edge expertise. This industry-linked R&D initiative is then providing an opportunity and creating tremendous educational value through students' participation. This also serves to upgrade faculty skills leading to new teaching curriculum within post-secondary education institutions. DEMO therefore increases NSCC's capacity to work with industry on the barriers obstructing the uptake of marine operations in high flow tidal environments. By being able to address these difficulties, companies will be well-positioned to develop competitive advantages in this sector, increasing their access to new clients and in some cases, increasing their margins through improved cost-effectiveness.

This report and part of the results are based on the work conducted using the Cougar ROV. However, the Cougar ROV from DDL was replaced by the Falcon Seaeye 12423 from the Ocean Tracking Network (OTN), due to DDL's withdrawal from the project. The simulation results were therefore only updated for the scenarios selected for testing in a controlled environment in the Aquatron facility at Dalhousie University.

II- TARGET SITE LOCATION FOR FIELD TESTING

The project intends to enhance marine operations capacity and efficiency in high flow environments, with applications at the Fundy Ocean Research Centre for Energy (FORCE)'s location. This site is located in the Minas Passage, a natural bottle-neck in the Bay of Fundy (Fig. 1), near Black Rock, 10 km west of Parrsboro, Nova Scotia (NS). Minas Passage, only 5 km wide and bordered by basalt cliffs, is the entrance to Minas Basin, the region of the world's highest tides, going over 16 meters. The tidal currents in this region are fast, exceeding 10 knots (5 m/s) at peak surface speed, making marine operations extremely challenging.



Figure 1: FORCE site location.

III- EXPECTED MILESTONES

III-1- Work Package 1 (Phase #1):

Establish baseline capabilities of selected ROVs and sensors equipment to be tested in the Bay of Fundy. These capabilities will be established for the current marine renewable sites in the Digby and Minas Passage areas. NSCC will assess the technical feasibility of deploying an ROV in selected sites, based on Dominion Diving's marine assets and expertise to conduct testing in the Bay of Fundy and to develop the technology upgrade required to successfully complete this research program. Duration: 06 months.

III-2- Work Package 2 (Phase #2):

Develop modeling capabilities that apply the outcome of the previous phase toward developing a set of tools that will help reduce the risks associated with operations in high flow tidal

environments. The capabilities developed will also be used to assess optimization requirements to existing marine assets. This will build on expertise developed by the Heuristic and Evolutionary Algorithms Laboratory of the School of Informatics, Communications and Media of the University of Applied Sciences in Upper Austria (NSCC partner). Dynamic Systems Analysis Ltd. (DSA) will provide dynamic analysis software and expertise to assess the motions and loads on the proposed ROV configurations, to reduce operation risks in the Bay of Fundy high flow tidal environments. Duration: 16 months.

III-3- Work Package 3 (Phase #3):

Premobilization testing for design parameters and configuration validation. This will consist of preliminary testing and validation. An integrated approach in project coordination will be used at this stage and all partners will be involved. System's configuration will be refined as needed. Duration: 01 month.

III-4- Work Package 4 (Phase #4):

ROV trials in the Bay of Fundy. A brief summary of the planned activities is detailed below.

Premobilization activities

- Prepare documentation required for marine access permit application.
- Confirm all planned ROV mission scenarios for the trial program.
- Confirm all local environmental parameters/factors that will be monitored and recorded during the trials and confirm which equipment will be used.

Mobilization

- Mobilize Cougar XT Custom ROV system onto Dominion Victory.
- Mobilize all project specific equipment onto Dominion Victory.
- Conduct wet tests to confirm functionality of the ROV spread.

General onsite activities

- Vessel transit from Dartmouth to testing site.
- Vessel setup/anchoring trials.
- Basic ROV launch and recovery trials.
- If any of the above ROV trials is unsuccessful, conduct a performance improvement, then ROV tether and associated actions; repeat as necessary. This option relies on the vessel adjusting position to get the ROV at a desired location, which is achieved via controlled and coordinated movements between the vessel anchor wire and bow thruster.
- These trials will be conducted from areas of lower tide speed and moving toward areas of higher speed or more turbulent areas in the Bay of Fundy, as we gain more

information on what ROV configurations are yielding the best results for each specific task/trial.

Onsite trial #1: ROV only – Normal Umbilical

- Set up ROV (no skid) with normal free fly umbilical.
- Launch ROV and conduct planned trials to assess their feasibility. This will include: (i) Holding station on bottom; (ii) Holding station approximately 10 m off bottom; and (iii) Flying in straight line surveying the seabed (this will mimic future subsea asset inspection).
- The research team will establish how long the vehicle is able to conduct operations in the water, and what operations can be conducted successfully with this configuration during a slack tide.
- Recover ROV to deck.
- Repeat any of above as needed and conduct a nondestructive inspection of all components.

Onsite trial #2: ROV & Dual Arm Skid – Normal Umbilical

- Set up ROV with dual arm skid and normal free fly umbilical.
- Launch ROV and conduct planned trials to assess their feasibility. This will include: (i) Holding station on bottom; (ii) Holding station approximately 10 m off bottom; (iii) Flying in straight line surveying the seabed (this will mimic future subsea asset inspection); and (iv) Holding station approximately 10m off bottom and mimic future subsea asset intervention.
- The research team will determine how long the vehicle is able to conduct operations in the water, and what operations can be conducted successfully with this configuration during a slack tide.
- Recover ROV to deck.
- Repeat any of above as needed and conduct a nondestructive inspection of all components.

Onsite trial #3: ROV & Ballast Skid – Normal Umbilical

- Set up ROV with ballast skid and normal free fly umbilical.
- All other steps as described on trial #1

Onsite trial #4: ROV & Dual Arm Skid – Armored Umbilical

- Set up ROV with dual arm skid and heavy duty armoured umbilical.
- Launch ROV and conduct planned trials to assess their feasibility. This will include: (i) Holding station on bottom; (ii) Flying in straight line surveying the seabed (this will

- mimic future subsea asset inspection); and (iii) Holding station approximately 10m off bottom and mimic future subsea asset intervention.
- All other steps as described previously.

Onsite trial #5: ROV & Ballast Skid – Armored Umbilical

- Set up ROV with ballast skid and heavy duty armoured umbilical.
- Launch ROV and conduct planned trials to assess their feasibility. This will include: (i) Holding station on bottom; and (ii) Flying in straight line surveying the seabed (this will mimic future subsea asset inspection).
- All other steps as described previously.

Demobilization / Close Out

This will include: (i) Transit from testing site to Dartmouth; (ii) Demobilize all equipment from Dominion Victory; (iii) Onshore postprocessing/analysis of collected data; (iv) Lessons learned; and (v) Reporting.

Duration: 01 month.

III-5- Important update

These expected milestones were updated during the course of the project, due to logistics limitation for conducting testing in the Bay of Fundy. Work Package 4 (Phase #4) was then cancelled and replaced with testing in a controlled environment, the Aquatron facility at Dalhousie University.

IV- ROV AND UMBILICAL MODELING

IV-1- Reference frames

In general, the ROV-umbilical system can be defined by two reference coordinate systems. One coordinate system is fixed relative to earth (global coordinate) and one can be fixed with respect to the umbilical (local coordinate). Following the discretization of the finite element approach a total number of $N+1$ local coordinate systems could be used, N being the number of elements the umbilical is divided into. In other words, each node will have a local coordinate system.

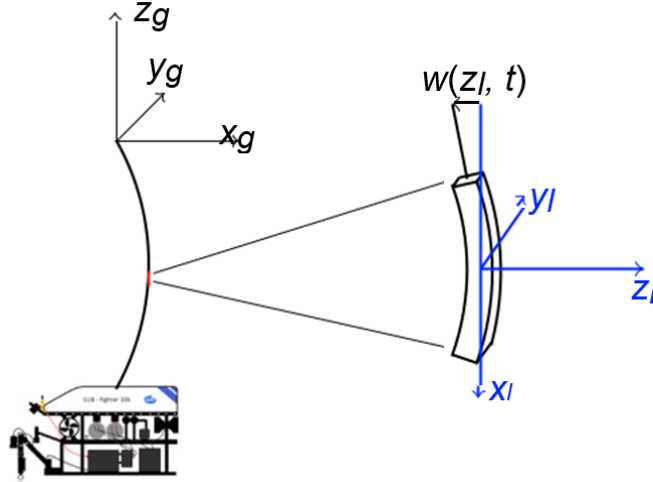


Figure 2: Reference frames for ROV-Umbilical model.

IV-2- Umbilical governing equations

The umbilical is developed in 3-dimensional space; hence 3 governing equations are used. The longitudinal equation of motion for a beam with uniform cross-section can be described as¹:

$$S + \frac{\partial S}{\partial x} dx - S - \rho A dx \frac{\partial^2 u}{\partial t^2} = 0 \quad (1)$$

where S is the internal axial stress resultant on the cross-section at a point x on the beam, u denotes the deflection, ρ denotes the mass density and A is the area of the cross-section. Using Hookes law the equation can be rewritten as:

$$EA \frac{\partial^2 u}{\partial x^2} = \rho A \frac{\partial^2 u}{\partial t^2} \quad (2)$$

The transverse equation of motion in y -direction is obtained from Euler-Bernoulli beam theory as:

$$\frac{\partial^2}{\partial x^2} \left(EI_y \frac{\partial^2 v}{\partial x^2} \right) + \rho A \frac{\partial^2 v}{\partial t^2} = F_y(x) \quad (3)$$

where $F_y(x)$ represents the external load and I_y is the second moment of inertia with regards to the y -axis. Similarly, the equation in z -direction becomes:

$$\frac{\partial^2}{\partial x^2} \left(EI_z \frac{\partial^2 w}{\partial x^2} \right) + \rho A \frac{\partial^2 w}{\partial t^2} = F_z(x) \quad (4)$$

For a ROV-umbilical the bending stiffness will be low and a certain amount of top-tension can be applied to reduce deflections. Because of testing in a shallow tank condition, the top-tension will be neglected and no further consideration will be given to this aspect.

IV-3- Umbilical boundary conditions

The initial configuration of the cable, as well as boundary conditions are as follows:

¹ Weaver Jr., W., Timoshenko, S.P., and Young, D. (1974). *Vibration problems in engineering. John Wiley & Sons Inc.*

$$u(0) = v(0) = w(0) = 0 \quad (5)$$

$$u(L) = u_{rov} - v(L) = v_{rov} - w(L) = w_{rov} \quad (6)$$

The torsional degree of freedom (i.e. rotation around the local x-axis) is neglected for the umbilical. This is done because the torsional rigidity is very small due to the large length-to-width ratio and of little interest in the umbilical modeling (hence total DOFs for each beam element is reduced from 12 to 10). For the ROV on the other hand all 6 degrees of freedom are of interest. The ROV is therefore modeled using all 6 degrees of freedom. The velocity and position of the ROV is denoted according to SNAME notation².

The top node is assumed to have a moment-free connection (simply supported, for example to a vessel). The other end of the umbilical is connected to the ROV. The umbilical is assumed to be connected to the ROV in the center of gravity which is also assumed to be the center of rotation. We therefore assume the end node to have the same position as the ROV (Figure 3). The node connected to the ROV is also assumed to be moment-free. Since the boundary nodes are moment-free i.e. no bending moment, the degrees of freedom at the boundaries are reduced from 10 to 6.

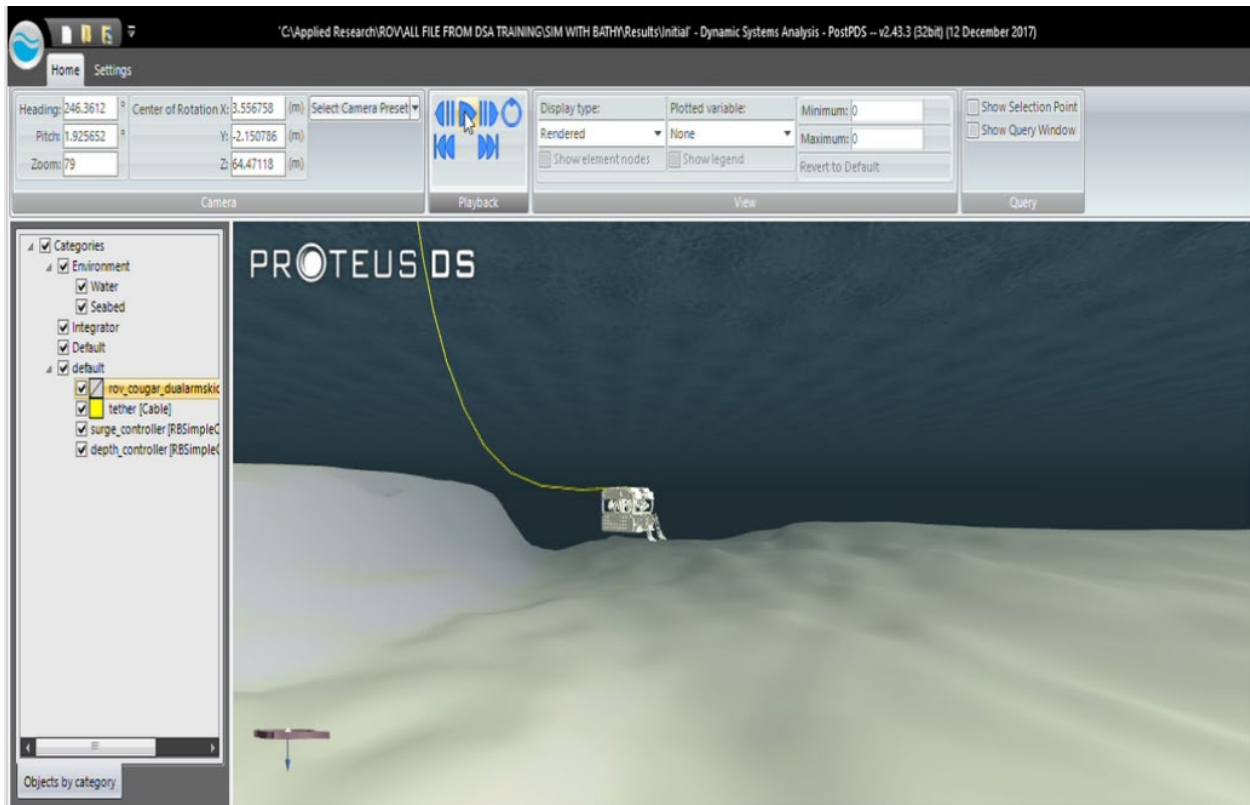


Figure 3: Illustration of the ROV + umbilical in the ProteusDS software.

² Fossen, T.I. (2011). Guidance and Control of Ocean Vehicles. John Wiley & sons, West Sussex, England, 1st. edition.

IV-4 Umbilical external loads

For a neutrally buoyant ROV-umbilical submerged in water the external loads are usually divided into three main contributions:

- Ship loads
- ROV loads
- Environmental loads

The ship loads are connected to the boundary conditions at the top-end of the umbilical and are assumed to be zero, from the previous subsection. The ROV loads are connected to the bottom-end of the umbilical and may consist of three contributions:

- Mass and added mass due to ROV acceleration;
- Hydrodynamic damping due to the ROV velocity relative to the incident current; and
- Thruster forces.

The present report will only focus on the thruster forces.

The environmental loads generally consist of current loads (drag forces) due to tide and wind. Wave forces are neglected as they will not contribute to a mean force on the umbilical, at this stage of tank testing in a controlled environment. As such, there is no need for transformations between the local element-reference frames and the global reference frame (Fig # coordinate syst). Current velocity is assumed to be constant in time.

IV-5- ROV governing equation

The ROV is modeled in 6 degrees of freedom (Fossen,2011) by :

$$(M + M_A)\dot{v} + (C(v_r) + C_A(v_r))v_r + K(v_r)v_r + g(\mu) = \tau \quad (7)$$

It should be noticed that as the relative velocity v_r is used in Eq.7, the current velocity and therefore the current forces are included using superposition. Wave-forces are, as mentioned earlier not included in the modeling of the umbilical. The effect of the umbilical has therefore not been considered for testing in the Aquatron Pool Tank due to the limited allowable depth and the availability of one jet outlet affecting an insignificant portion of the umbilical.

V- COMPUTER-AIDED DESIGN (CAD) MODELING, MESHING AND SIMULATION

V-1- CAD modeling and meshing

To generate the results, a 3D CAD model as well as a mesh of the ROV were developed as shown in Figure 4 below. The modeling of the ROV was done in Inventor Professional 2018. Altair Hypermesh was used to create the .obj and mesh file formats used in ProteusDS. The CAD assembly file was first converted to IGS file format. The .igs file was then imported into Altair Hypermesh. All units were set to meters (m), as Hypermesh is a unitless software; this avoids

unwanted scaling of the part and all imported parts should be in units of m. The ROV parts were then meshed using Hypermesh.

Due to the complex geometries and sizes of the ROV parts, a careful meshing approach was used where firstly, a general whole-body automatic mesh was created. An initial rough mesh size of 0.10 m including both triangular and quadrilateral surface mesh was used. A surface mesh type was chosen because the drag forces experienced by the ROV are only a function of external geometry. Therefore, any internal mesh is unnecessary and will also make the meshing process significantly more computationally demanding. This mesh size caused a lot of meshing errors because of the fine and small geometrical parts on the ROV such as thruster blades and sensors mounted onto the ROV. To solve this problem, all internal parts and external parts that were judged to not contribute significantly to the overall drag effect of the ROV were deleted from the CAD file before being imported in Hypermesh. This greatly reduced the mesh creation time without any important loss in geometrical or mass effect in the subsequent simulations.

A picture of the ROV used in Trial 1 can be seen in Figure 4. The mesh size was further reduced to 0.01 m. This was done to capture the geometry of the thrusters. A special script provided by Altair was used to convert the meshed ROV into .obj file format. This .obj file format was then imported into proteusDS where initial test simulation trials were run. Due to the fine size of the mesh, the simulations in proteusDS were overly computationally demanding with each simulation time of around 10 days or plus to complete. Given the time constraint, this was not a viable option to explore. The meshed ROV was then replaced with a cuboid of equivalent surface area. All subsequent simulations were performed using cuboids of the ROV or ROV with Dual Arm dimensions. These dimensions are given in Tables 1 and 2. The Meshed ROV was only used for visualization and presentation purposes in ProteusDS.

A simulation of the meshed ROV was set up and ran with a very small simulation time of 0.1 second. This is just enough for ProteusDS to calculate the mesh surface area. The output file was then exported to an excel file where linear regression was done and the approximate size of the ROV was obtained. Data were generated assuming that the system is kinematically fixed.

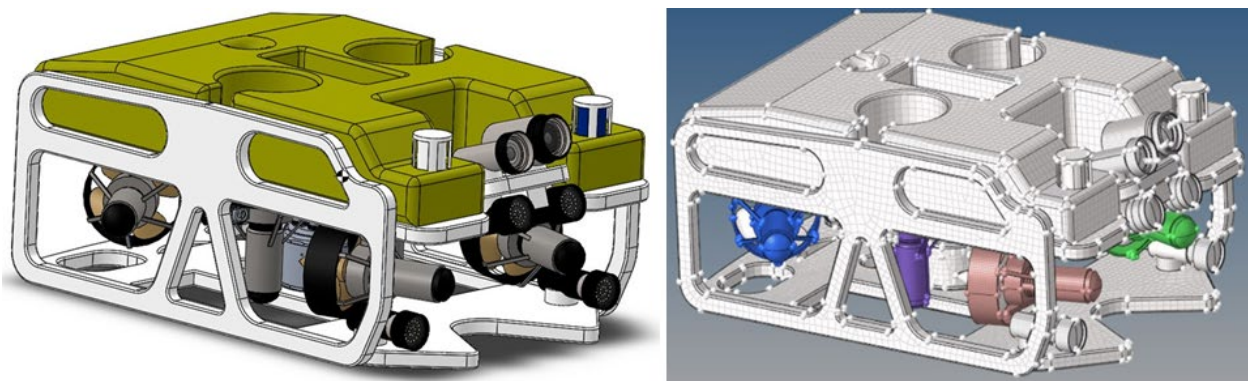


Figure 4: 3D CAD model (left) and meshing (right) of the Cougar XT-1420.

V-2- Simulation data generation

Work Package 1

Trial #2

A normal umbilical cord was used in the simulation, which has a 1 inch diameter (Figure 5).

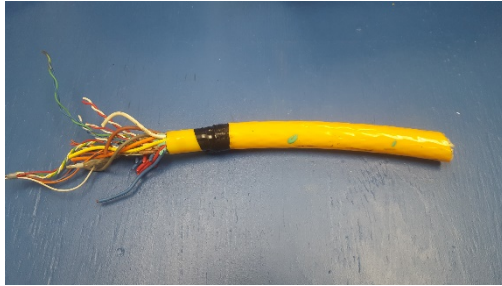


Figure 5: Normal umbilical cord (1 inch diameter).

Data were obtained as presented in below.

Holding Station on Bottom

The horizontal reaction loads plot at 75 m depth and 0 heading is given in Figure 6 below, showing that the lateral thruster (capacity = 1,510 N or 339.46 lbs) will perform safely up to a current speed of 1.50 m/s.

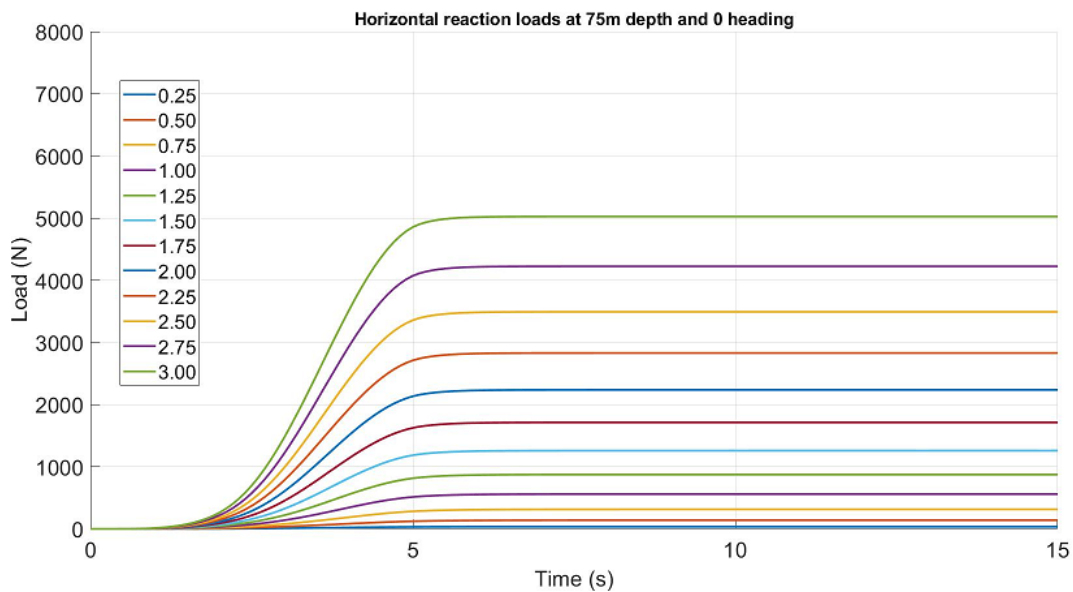


Figure 6: Horizontal reaction loads at 75 m depth and 0 heading

The horizontal reaction loads plot at 75 m depth and 90 heading is given in Figure 7 below, showing that the forward thruster (capacity = 2,000 N or 449.84 lbs) will perform safely up to a current speed of 2 m/s.

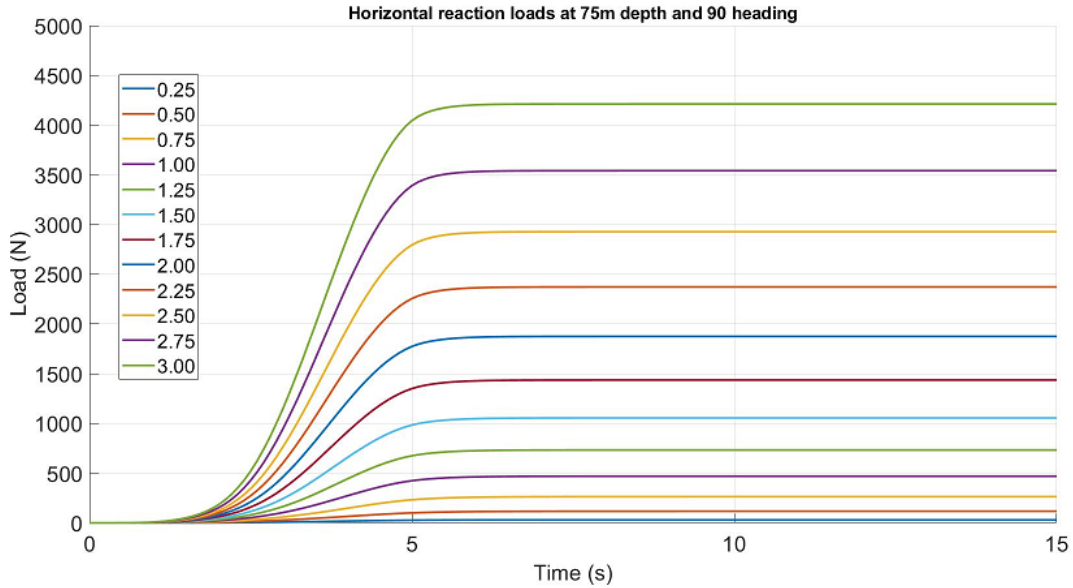


Figure 7: Horizontal reaction loads at 75 m depth and 90 heading.

The vertical reaction loads plot at 75 m depth and 0 heading is given in Figure 8 below, showing that the vertical thruster (capacity = 1,196 N or 268.87 lbs) will not perform at all in this environment.

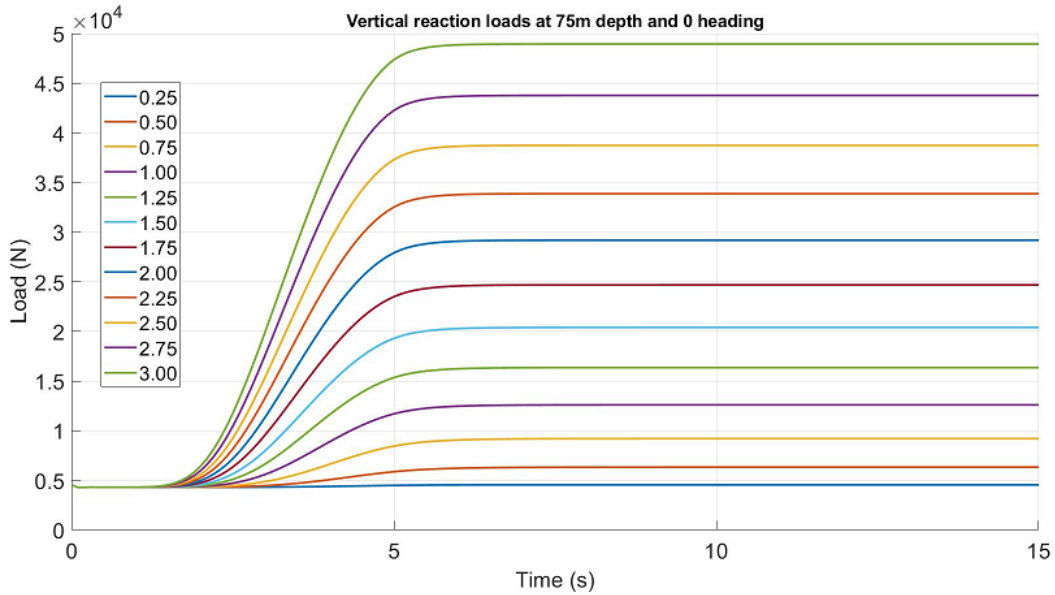


Figure 8: Vertical reaction loads at 75 m depth and 0 heading.

The vertical reaction loads plot at 75 m depth and 90 heading is given in Figure 9 below, showing that the vertical thruster (capacity = 1,196 N or 268.87 lbs) will not perform at all in this environment.

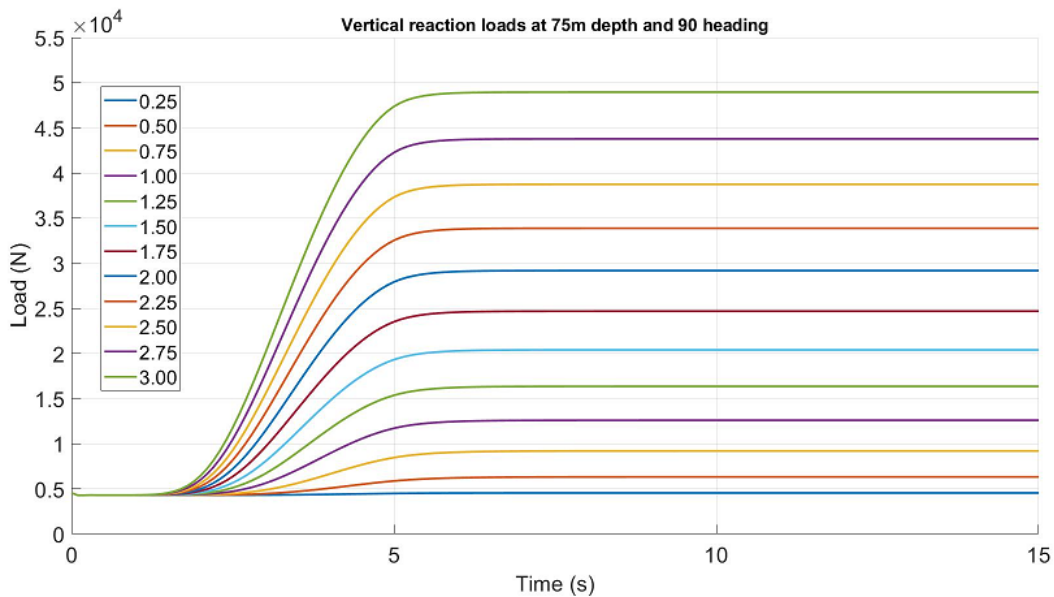


Figure 9: Vertical reaction loads at 75 m depth and 90 heading.

10 m off bottom

The horizontal reaction loads plot at 75 m depth and 0 heading is given in Figure 10 below, showing that the lateral thruster (capacity = 1,510 N or 339.46 lbs) will perform safely up to a current speed of 1.25 m/s.

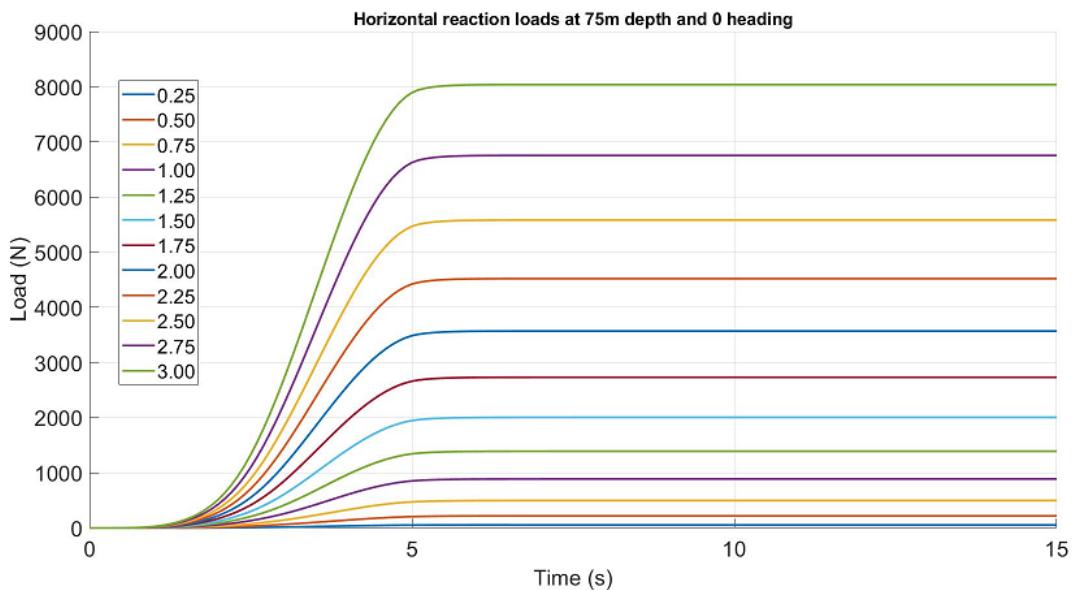


Figure 10: Horizontal reaction loads at 75 m depth and 0 heading.

The horizontal reaction loads plot at 75 m depth and 90 heading is given in Figure 11 below, showing that the forward thruster (capacity = 2,001 N or 449.84 lbs) will perform safely up to a current speed of 2 m/s.

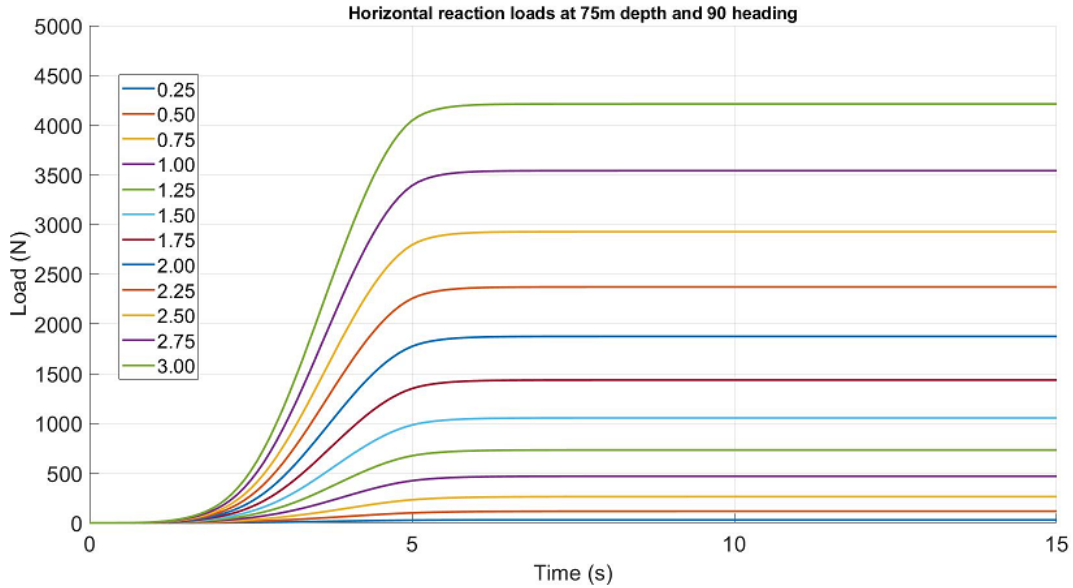


Figure 11: Horizontal reaction loads at 75 m depth and 90 heading.

The vertical reaction loads plot at 75 m depth and 0 heading is given in Figure 12 below, showing that the vertical thruster (capacity = 1,196 N or 268.87 lbs) will not perform at all in this environment.

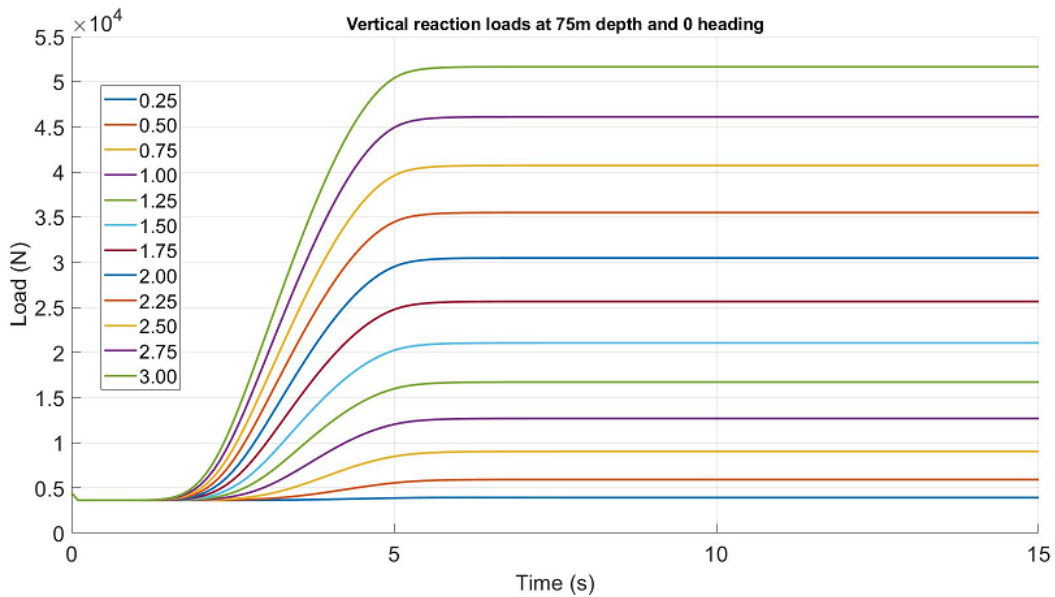


Figure 12: Vertical reaction loads at 75 m depth and 0 heading.

The vertical reaction loads plot at 75 m depth and 90 heading is given in Figure 13 below, showing that the vertical thruster (capacity = 1,196 N or 268.87 lbs) will not perform at all in this environment.

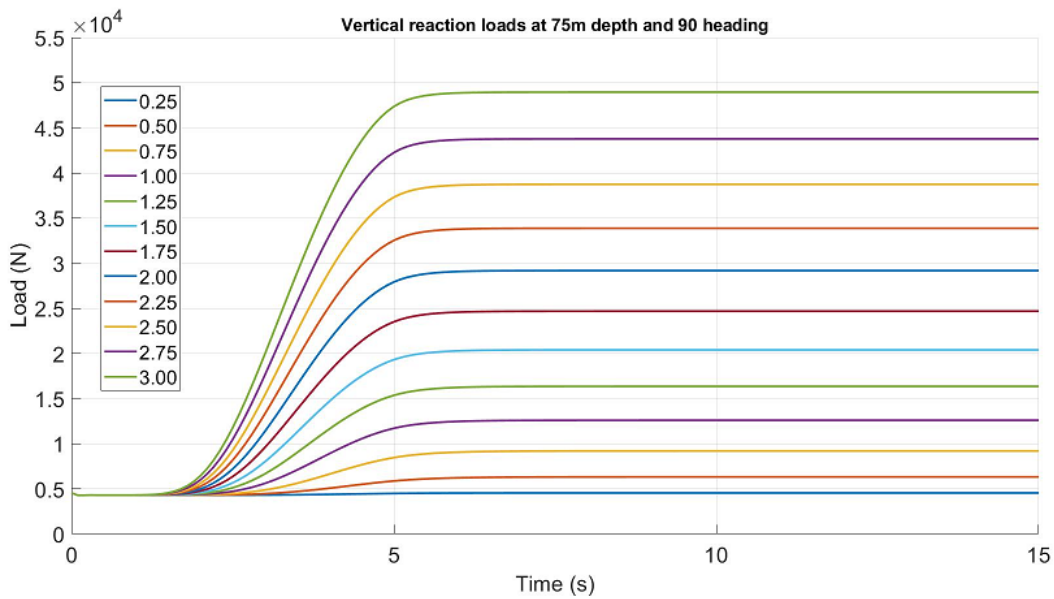


Figure 13: Vertical reaction loads at 75 m depth and 90 heading.

Trial #4

An armored umbilical cord was used in the simulation, which has a 1.49 inch diameter (Figure 14).



Figure 14: Armored umbilical cord (1.49 inch diameter).

Data were obtained as presented below.

Holding Station on Bottom

The horizontal reaction loads plot at 75 m depth and 0 heading is given in Figure 15 below, showing that the lateral thruster (capacity = 1,510 N or 339.46 lbs) will perform safely up to a current speed of 1.50 m/s.

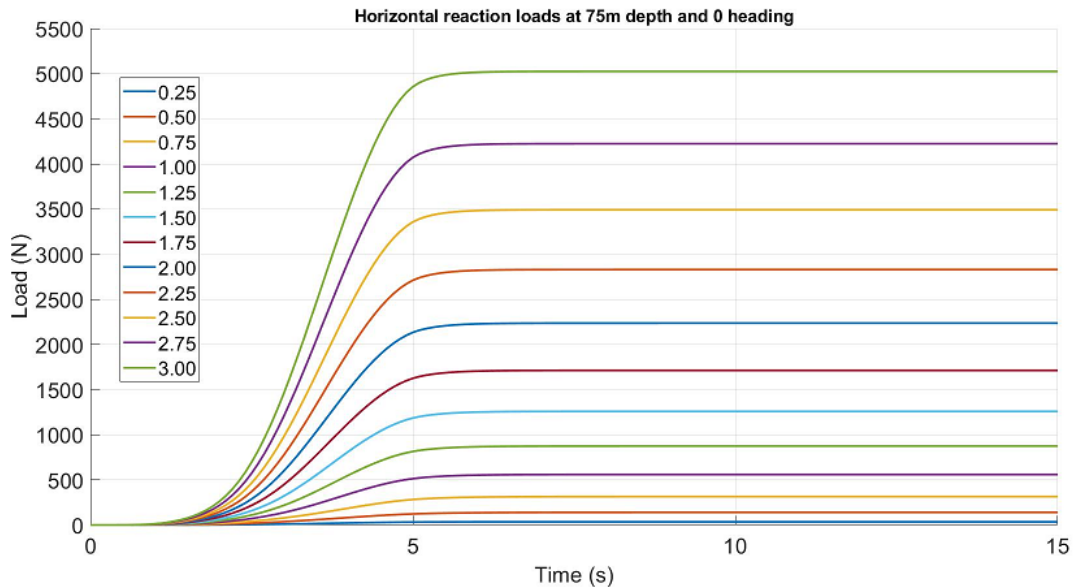


Figure 15: Horizontal reaction loads at 75 m depth and 0 heading.

The horizontal reaction loads plot at 75 m depth and 90 heading is given in Figure 16 below, showing that the forward thruster (capacity = 2,000 N or 449.84 lbs) will perform safely up to a current speed of 2 m/s.

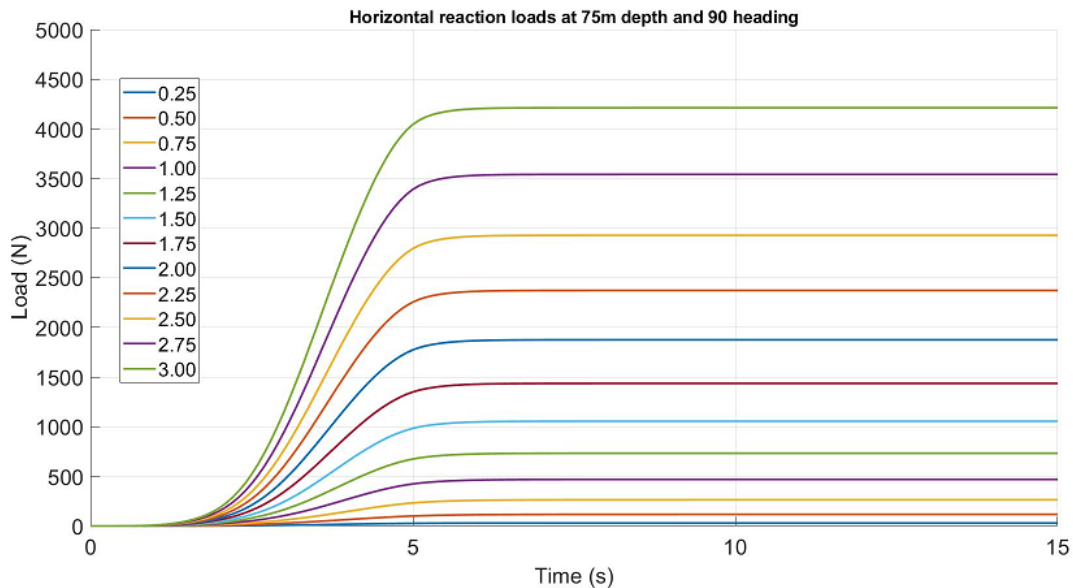


Figure 16: Horizontal reaction loads at 75 m depth and 90 heading.

The vertical reaction loads plot at 75 m depth and 0 heading is given in Figure 17 below, showing that the vertical thruster (capacity = 1,196 N or 268.87 lbs) will not perform at all in this environment.

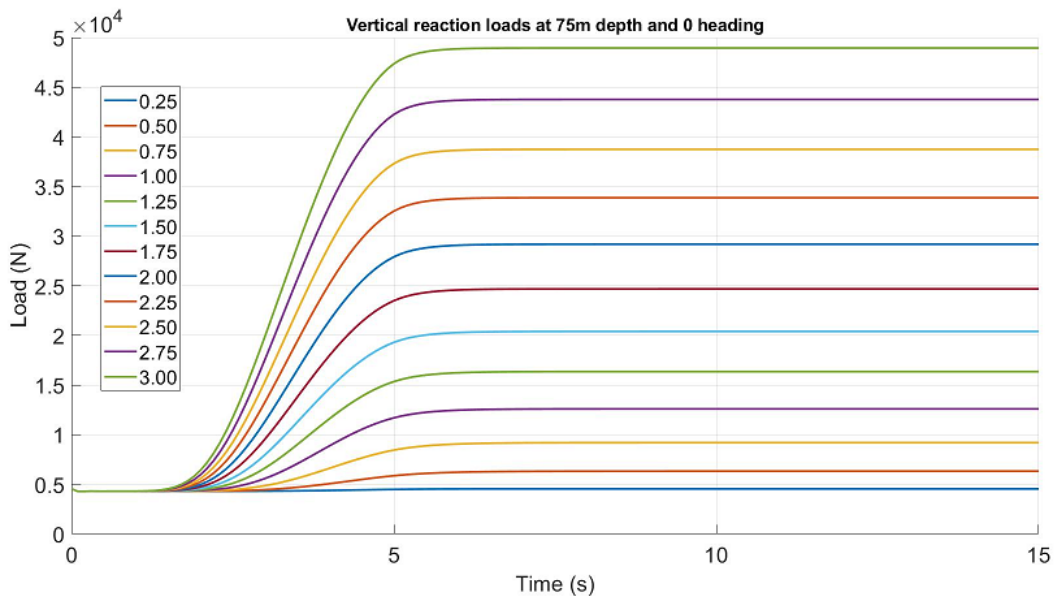


Figure 17: Vertical reaction loads at 75 m depth and 0 heading.

The vertical reaction loads plot at 75 m depth and 90 heading is given in Figure 18 below, showing that the vertical thruster (capacity = 1,196 N or 268.87 lbs) will not perform at all in this environment.

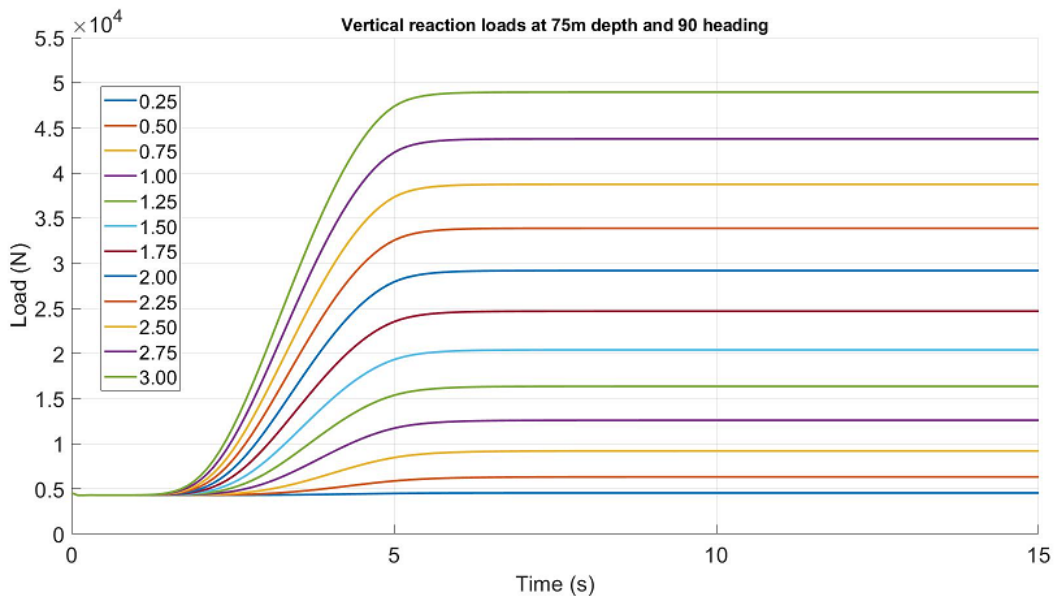


Figure 18: Vertical reaction loads at 75 m depth and 90 heading.

10 m off bottom

The horizontal reaction loads plot at 75 m depth and 0 heading is given in Figure 19 below, showing that the lateral thruster (capacity = 1,510 N or 339.46 lbs) will perform safely up to a current speed of 1.25 m/s.

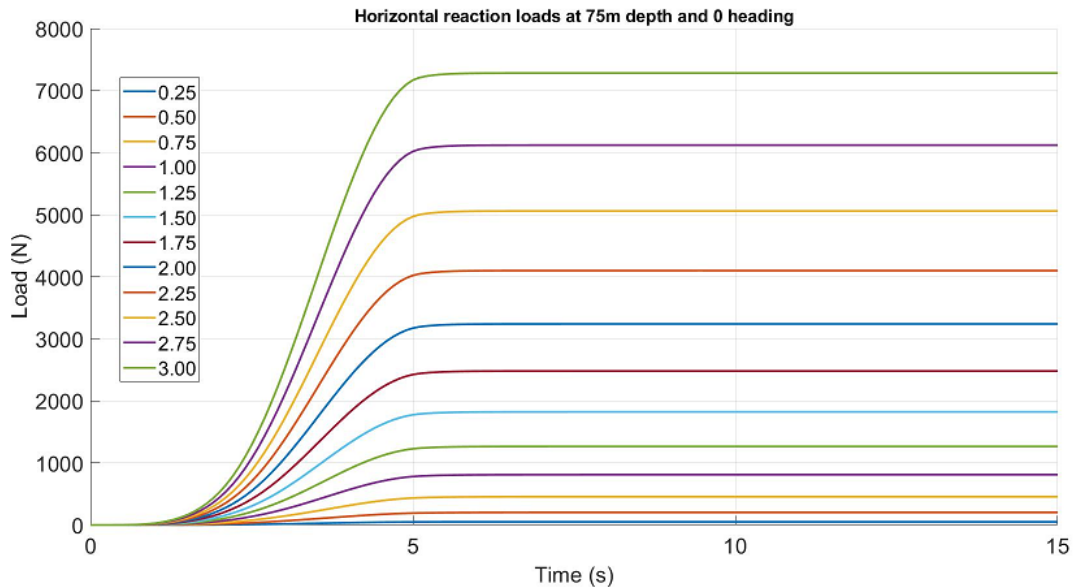


Figure 19: Horizontal reaction loads at 75 m depth and 0 heading.

The horizontal reaction loads plot at 75 m depth and 90 heading is given in Figure 20 below, showing that the forward thruster (capacity = 2,001 N or 449.84 lbs) will perform safely up to a current speed of 1.75 m/s.

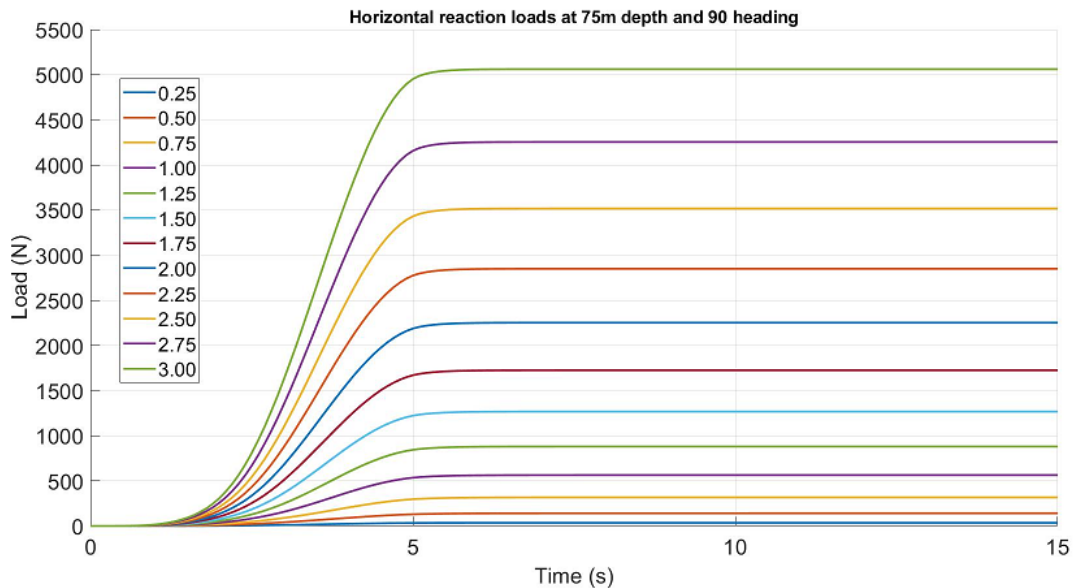


Figure 20: Horizontal reaction loads at 75 m depth and 90 heading.

The vertical reaction loads plot at 75 m depth and 0 heading is given in Figure 21 below, showing that the vertical thruster (capacity = 1,196 N or 268.87 lbs) will not perform at all in this environment.

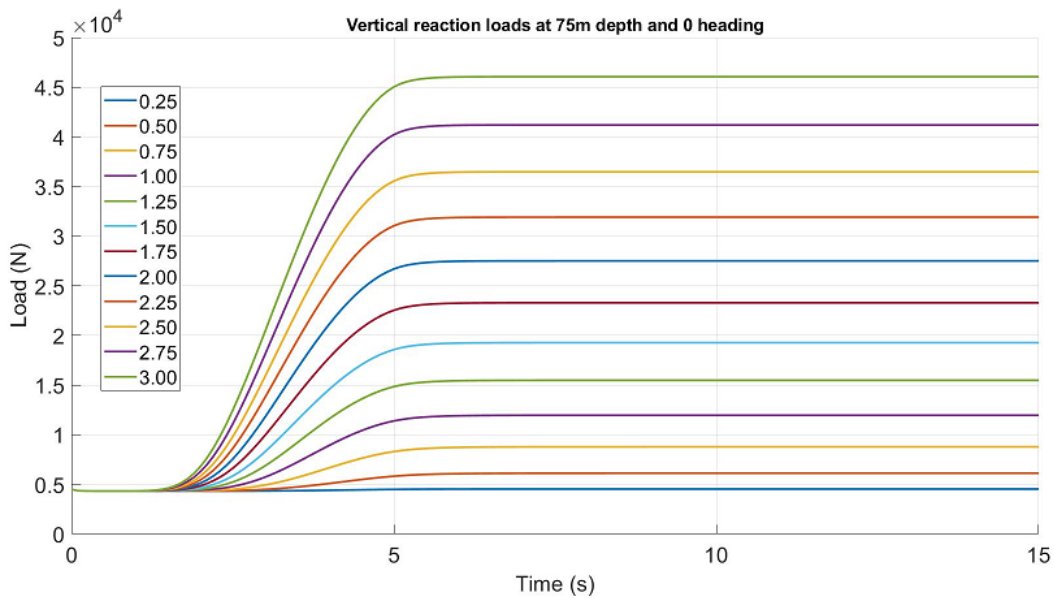


Figure 21: Vertical reaction loads at 75 m depth and 0 heading.

The vertical reaction loads plot at 75 m depth and 90 heading is given in Figure 22 below, showing that the vertical thruster (capacity = 1,196 N or 268.87 lbs) will not perform at all in this environment.

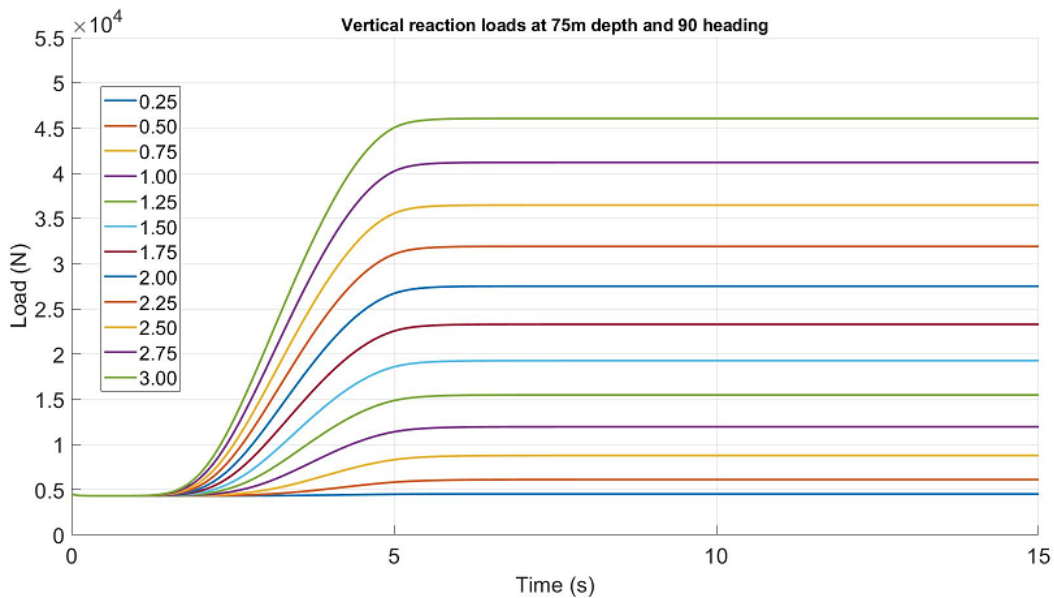


Figure 22: Vertical reaction loads at 75 m depth and 90 heading.

Work Package 2

This Work Package has focused on further generating simulation data for different deployment scenarios not addressed in Work Package 1 (trials #1, #3 and #5), using the ProteusDS modeling software (DSA Ltd.), a full-featured dynamic analysis software capable of simulating vessels, flexible structures, lines and technologies in harsh marine environments. In the simulations the ROV was held in position on the seabed at 75m water depth. A 26mm diameter umbilical was attached to the ROV running up to the surface. Once the static thruster requirements were established, the ROV was then held at 10m off bottom, thrusters' capabilities were revisited. The combined drag forces on the ROV and the umbilical were used to assess the thruster requirements to hold that position under several current speeds.

The results on trials #3 and #5 were like those of trials #2 and #4 above. The simulation data generated are presented in Figures 23 to 34.

10m off the bottom

The horizontal reaction loads plot at 10m off the bottom and 0° heading is given in Figure 23 below, showing that the forward thruster (capacity = 2,000 N or 449.84 lbs) will perform safely up to a current speed of 1.5 m/s.

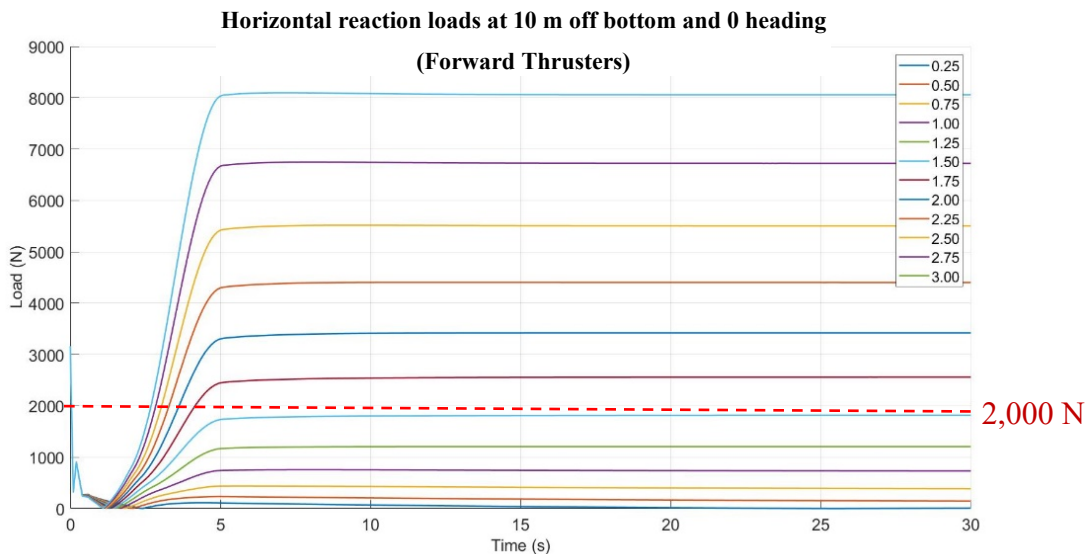


Figure 23: 10m off the bottom, kinematically fixed – Horizontal Reaction Loads, 0° Heading (forward thrusters).

The horizontal reaction loads plot at 10 m off the bottom and 0° heading is given in Figure 24 below, showing that the lateral thruster (capacity = 1,510 N or 339.46 lbs) will perform safely at all currents. The lateral forces for this configuration are negligible.

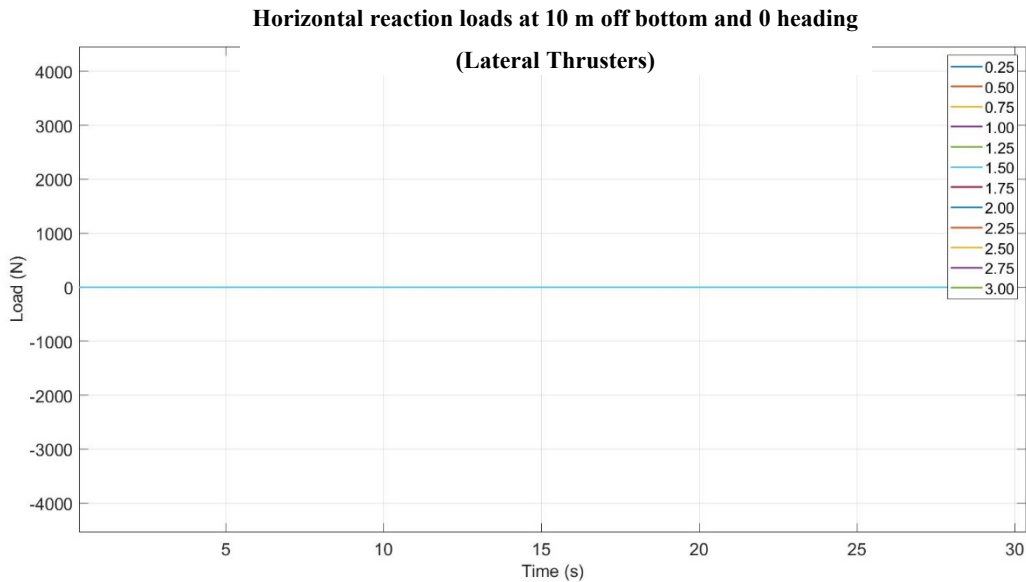


Figure 24: 10m off the bottom, kinematically fixed – Horizontal Reaction Loads, 0° Heading (lateral thrusters).

The horizontal reaction loads plot at 10m off the bottom and 90° heading is given in Figure 25 below, showing that the forward thruster (capacity = 2,000 N or 449.84 lbs) will perform safely at all speeds. The forward forces for this configuration are negligible.

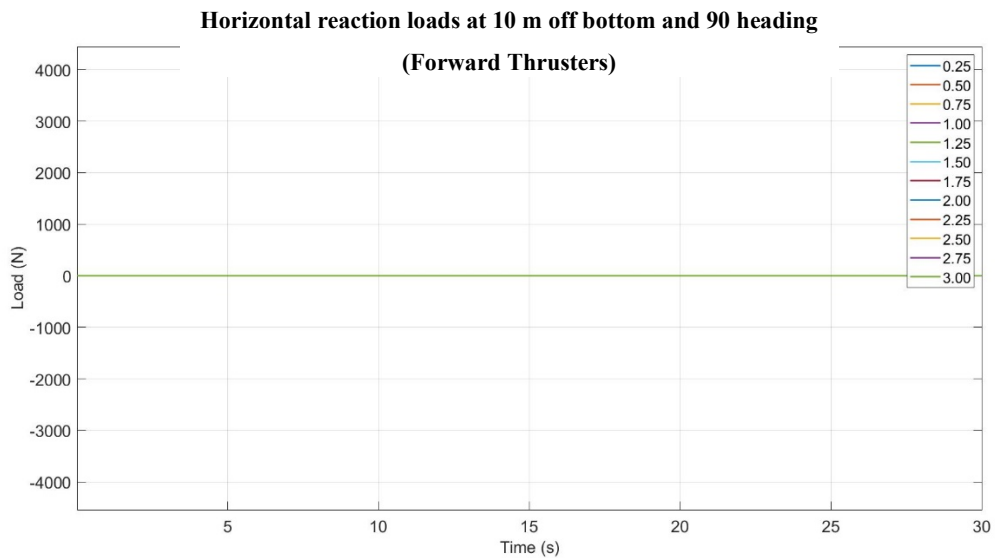


Figure 25: 10m off the bottom, kinematically fixed – Horizontal Reaction Loads, 90° Heading (forward thrusters).

The horizontal reaction loads plot at 10m off the bottom and 90° heading is given in Figure 26 below, showing that the lateral thruster (capacity = 1,510 N or 339.46 lbs) will perform safely up to current speed of about 1.25 m/s.

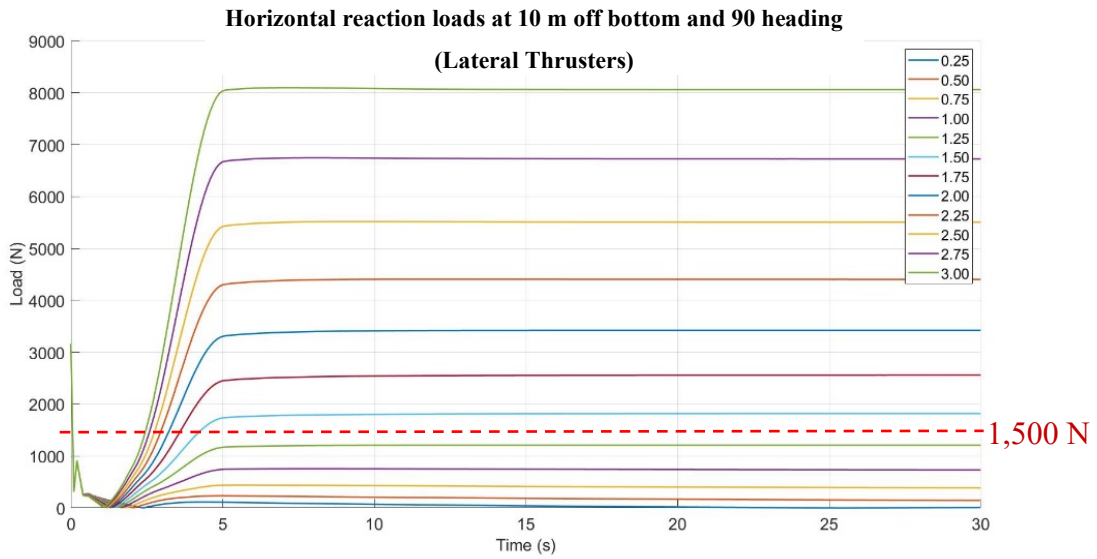


Figure 26: 10m off the bottom, kinematically fixed – Horizontal Reaction Loads, 90° Heading (lateral thrusters).

The vertical reaction loads plot at 10 m off the bottom and 0 heading is given in Figure 27 below, showing that the vertical thruster (capacity = 1,196 N or 268.87 lbs) will perform safely up to current speed of about 2.25 m/s.

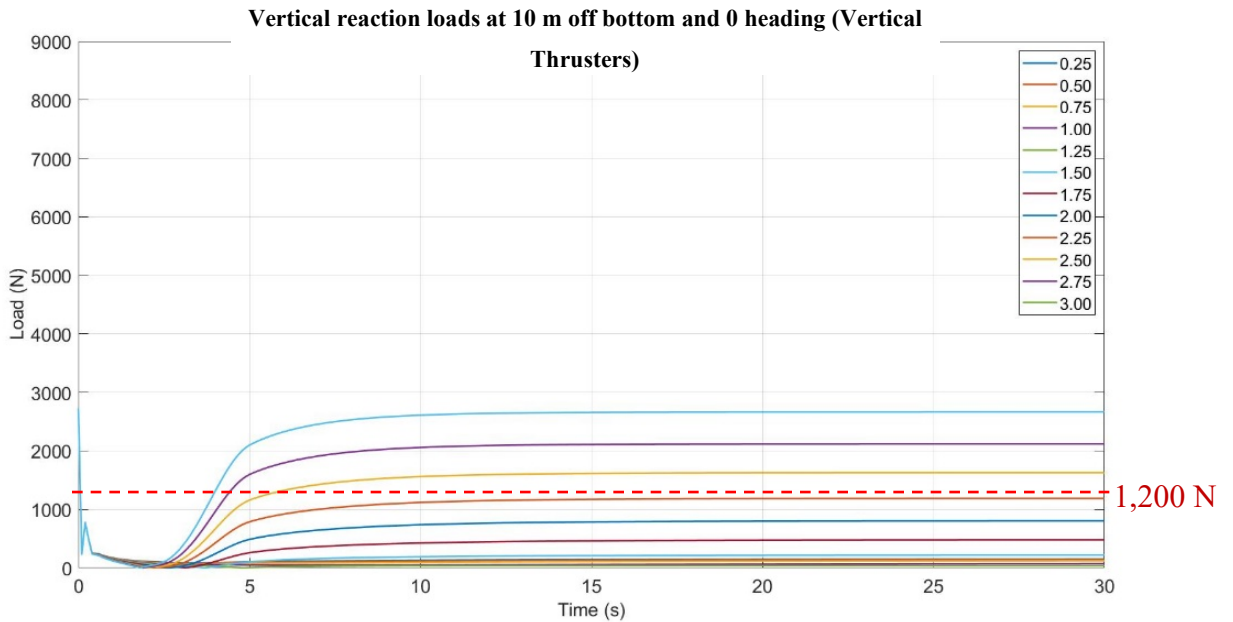


Figure 27: 10m off the bottom, kinematically fixed – Vertical Reaction Loads, 0° Heading (vertical thrusters).

The vertical reaction loads plot at 10 m off the bottom and 90° heading is given in Figure 28 below, showing that the vertical thruster (capacity = 1,196 N or 268.87 lbs) will perform safely up to current speed of about 2.25 m/s.

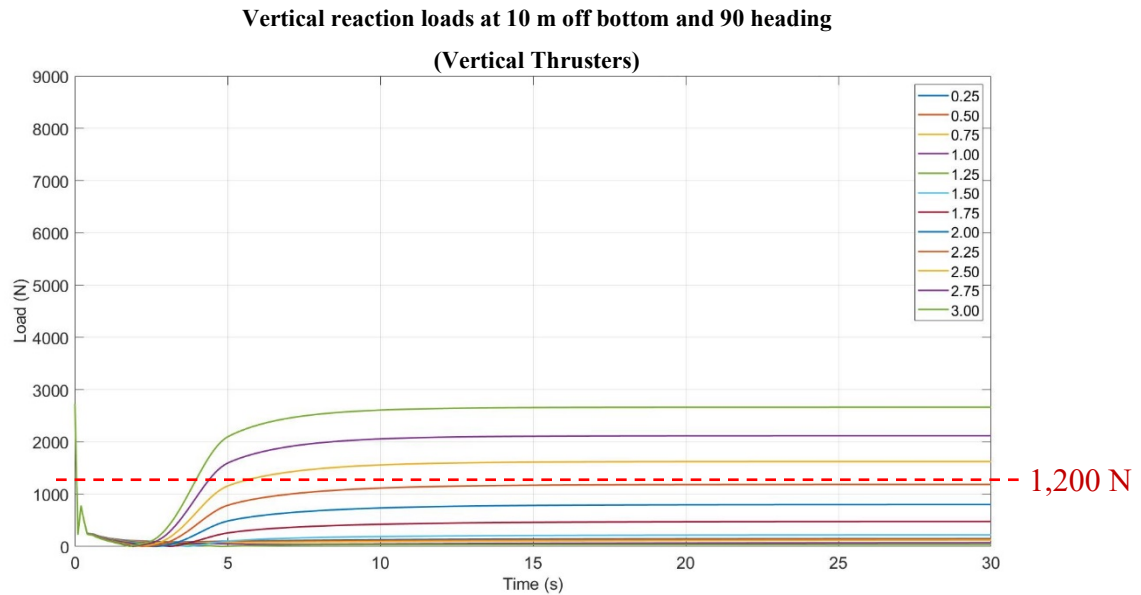


Figure 28: 10m off the bottom, kinematically fixed – Vertical Reaction Loads, 90° Heading (vertical thrusters).

Holding Station on Bottom

The horizontal reaction loads plot holding station on bottom and 0° heading is given in Figure 29 below, showing that the forward thruster (capacity = 2,000 N or 449.84 lbs) will perform safely up to a current speed of 1.75 m/s.

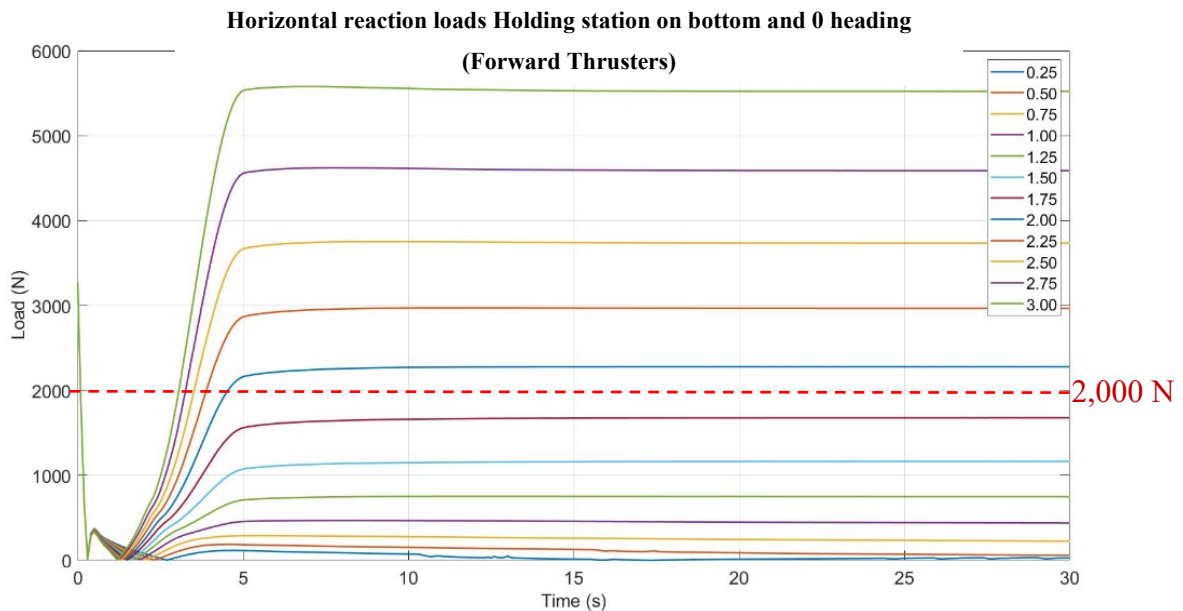


Figure 29: Holding station on bottom, kinematically fixed – Horizontal Reaction Loads, 0° Heading (forward thrusters).

The horizontal reaction loads plot for holding station on bottom and 0° heading is given in Figure 30 below, showing that the lateral thruster (capacity = 1,510 N or 339.46 lbs) will perform safely at all speeds. The lateral forces in this configuration are negligible.

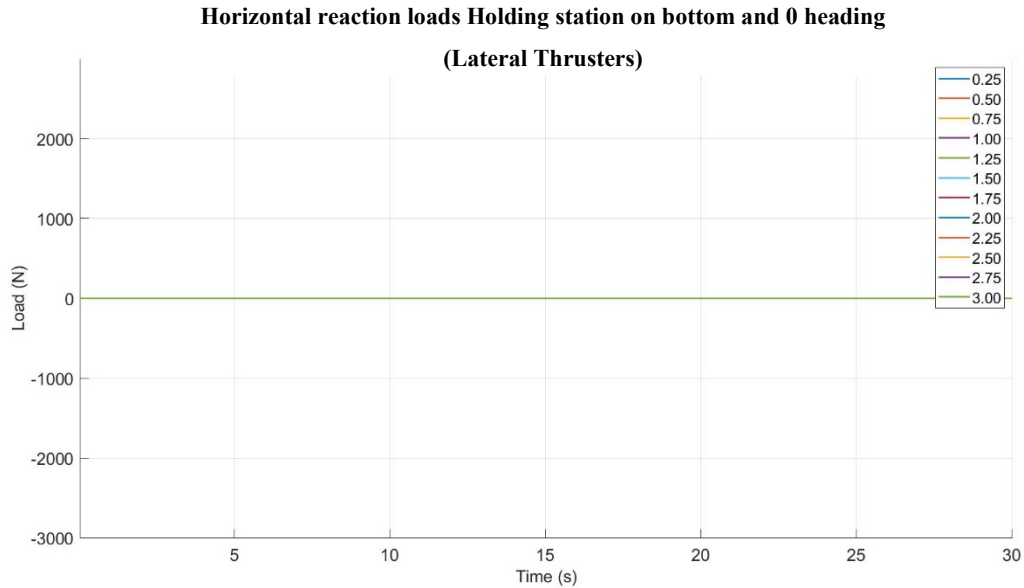


Figure 30: Holding station on bottom, kinematically fixed – Horizontal Reaction Loads, 0° Heading (lateral thrusters).

The horizontal reaction loads plot for holding station on bottom and 90° heading is given in Figure 31 below, showing that the forward thruster (capacity = 2,000 N or 449.84 lbs) will perform safely for all currents. The forward forces for this configuration are negligible.

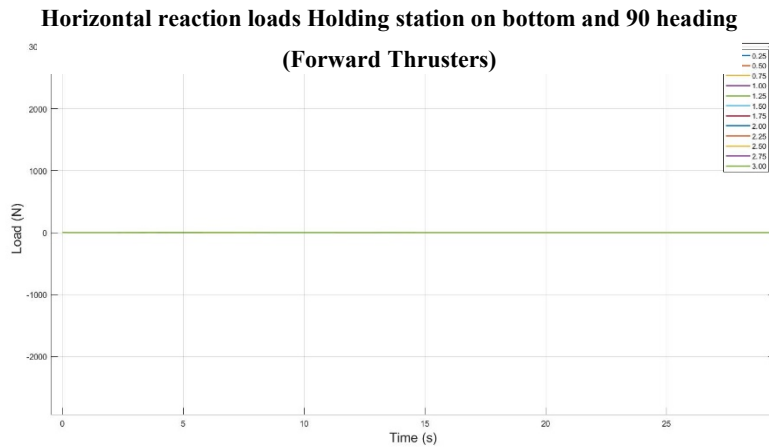


Figure 31: Holding station on bottom, kinematically fixed – Horizontal Reaction Loads, 90° Heading (forward thrusters).

The horizontal reaction loads plot for holding station on bottom and 90° heading is given in Figure 32 below, showing that the lateral thruster (capacity = 1,510 N or 339.46 lbs) will perform safely up to a current speed of 1.75 m/s.

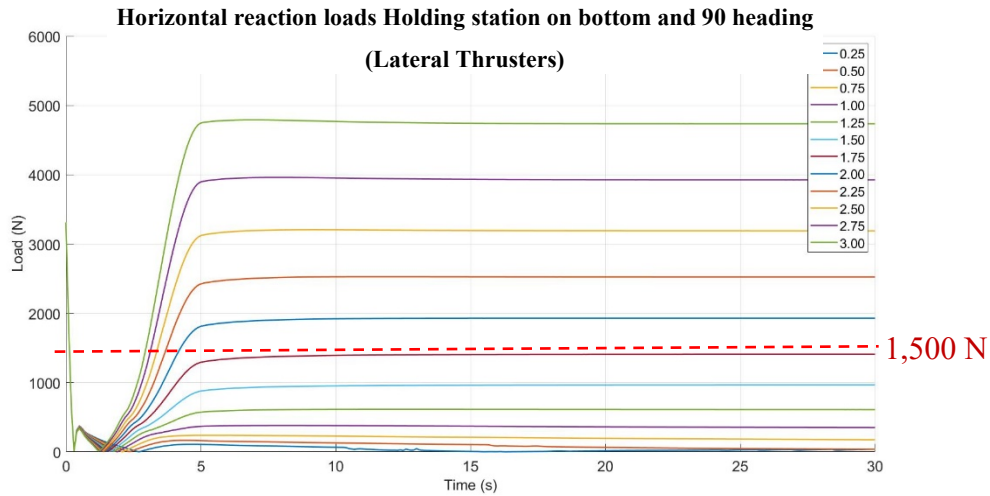


Figure 32: Holding station on bottom, kinematically fixed – Horizontal Reaction Loads, 90° Heading (lateral thrusters).

The vertical reaction loads plot for holding on bottom and 0° heading is given in Figure 33 below, showing that the vertical thruster (capacity = 1,196 N or 268.87 lbs) will perform safely up to current speed of about 2 m/s.

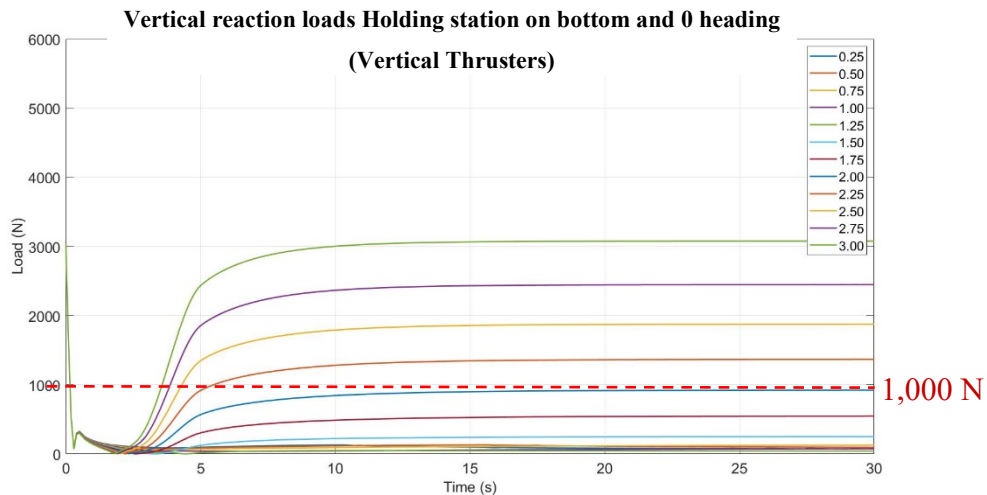


Figure 33: Holding station on bottom, kinematically fixed – Vertical Reaction Loads, 0° Heading (vertical thrusters).

The vertical reaction loads plot for holding on bottom and 90° heading is given in Figure 34 below, showing that the vertical thruster (capacity = 1,196 N or 268.87 lbs) will perform safely up to current speed of about 2 m/s.

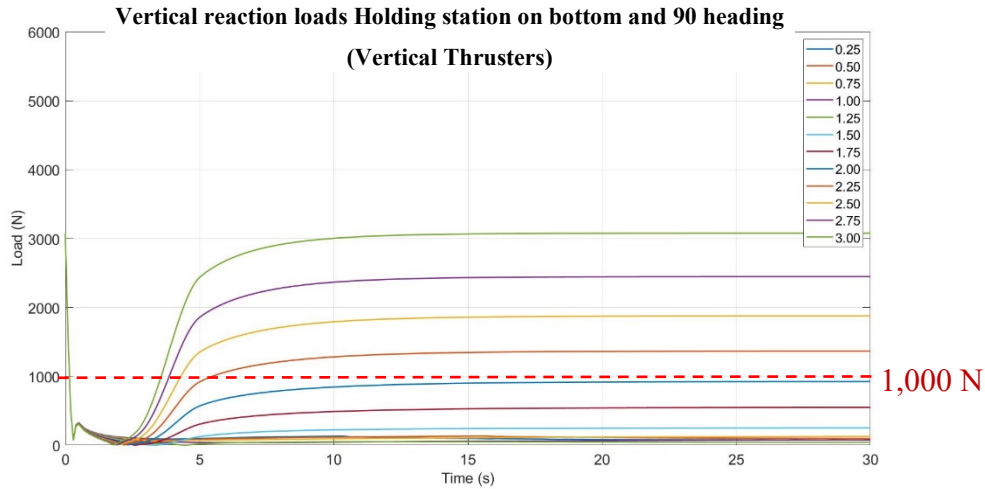


Figure 34: Holding station on bottom, kinematically fixed – Vertical Reaction Loads, 90° Heading (vertical thrusters).

VI- PLANNING EXPERIMENTAL VALIDATION OF SIMULATED RESULTS

VI-1- Approach used

This section represents Work Package 3 (Phase #3) of the project. Together with Dominion Diving, the research team has worked on preparing experimental protocol for a pre-deployment of the ROV at the Aquatron facility at Dalhousie University, housing a pool tank. This tank is 15.24m in diameter, 3.54m perimeter to 3.91m center, and 684,050 litres volume, made from reinforced concrete, and is deemed capable of serving as a site for deployment of the Cougar XT-1420 ROV in a controlled environment.

As an important factor for analytical data comparison is real value of the velocity vector and its components (V_x, V_y, V_z), the velocity matrix was determined by superimposing a coordinates net onto the tank measurement space with appropriate unit steps. Several nodes were obtained in the measurement space and the water velocity vector was estimated on these nodes. These data were obtained from Prof. Alex Hay’s experiment in the Aquatron, only on a plane in the water jet direction (see Figures 35-37 below). The resultant velocity matrix is key to calculations of experimental parameters to drive the ROV in the pool tank.

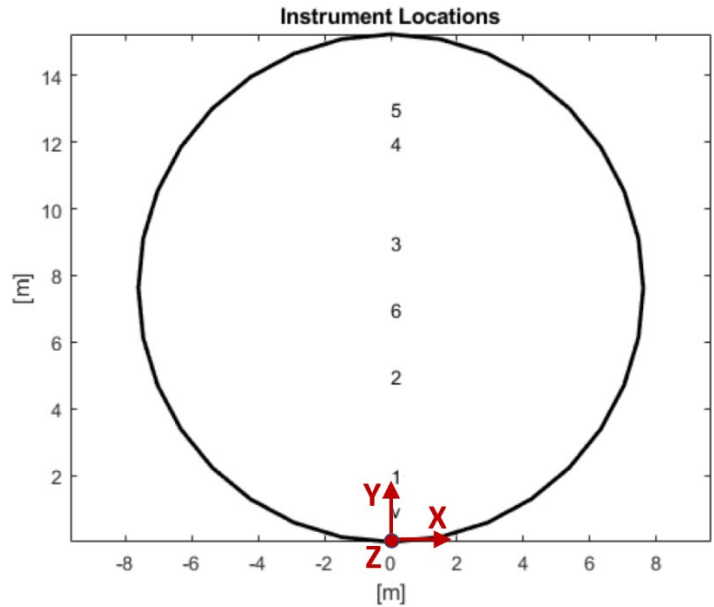


Figure 35. Plan view sketch of the pool tank showing the ADCP deployment positions. The Vectrino position is indicated by the “v”. [Aquatron Pool Tank Experiment: 22-25 January 2019 – OERA Interim Report by Prof. Alex Hay, Department of Oceanography, Dalhousie University].

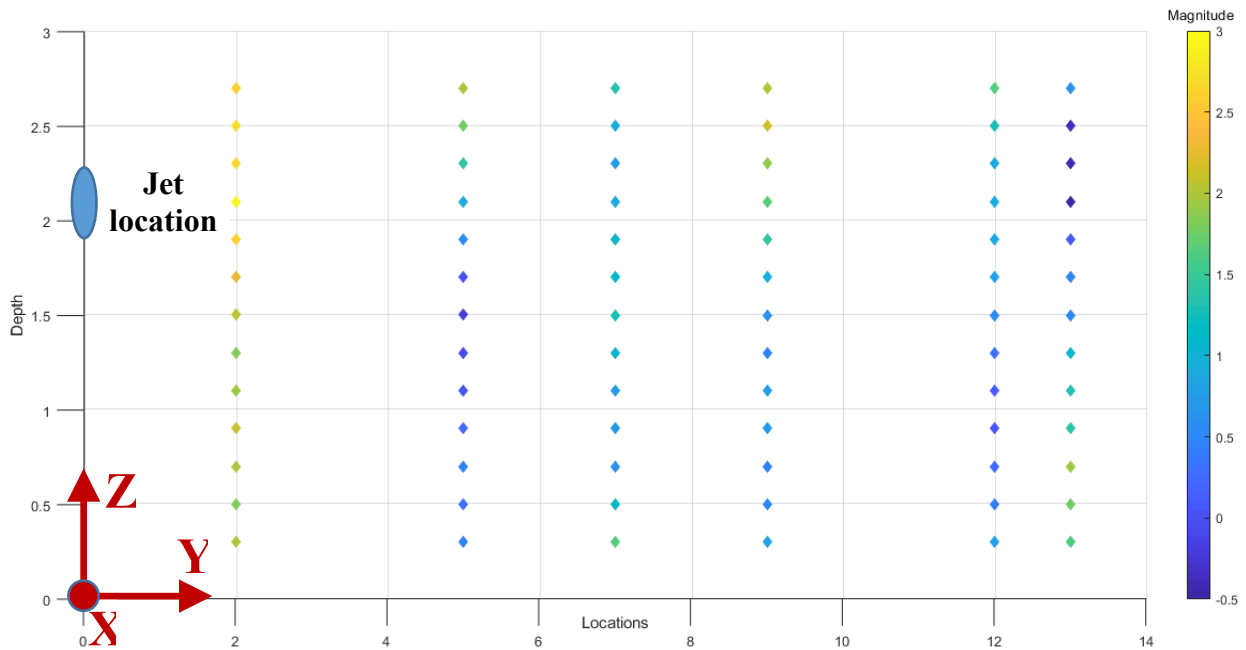


Figure 36. Plane view of the Aquatron velocity profile at 100% pump power at the positions shown in Fig. 14 along the Y-direction (V_y). The data was obtained by Prof. Alex Hay from the Department of Oceanography at Dalhousie University from the Aquatron Pool Tank Experiment: 22-25 January 2019.

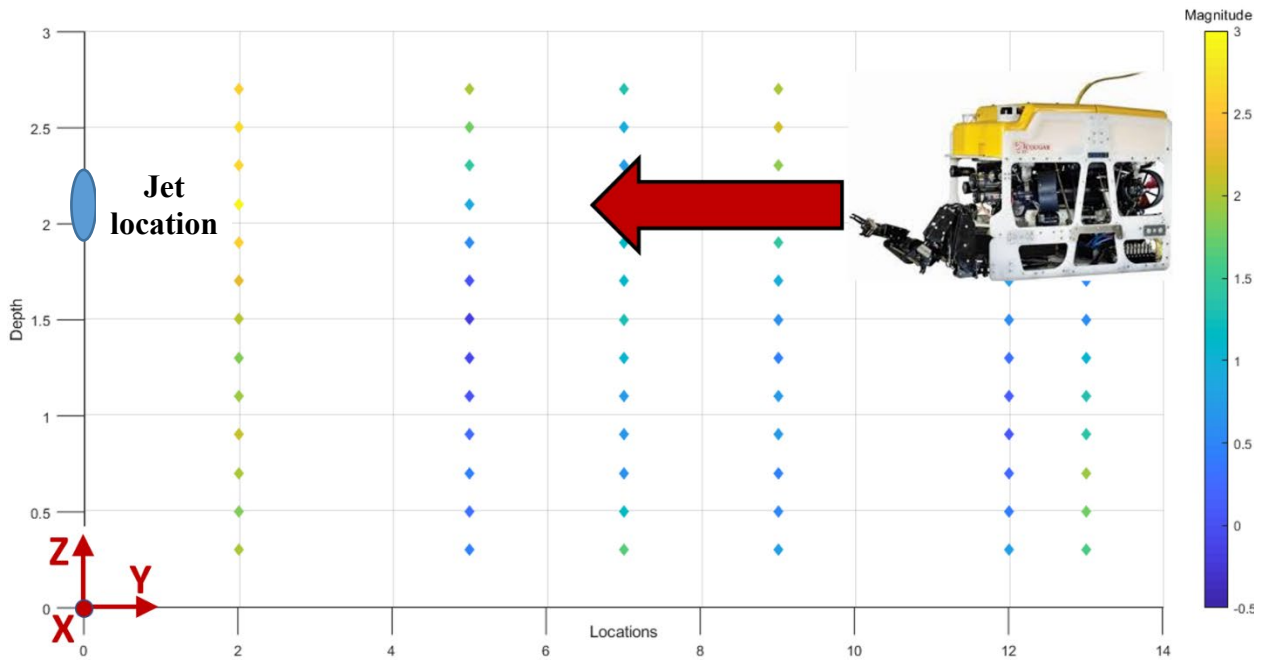


Figure 37. Illustration of the ROV starting location during the experiment to move to different positions towards the jet direction.

In preparation for the experimental validation at the Aquatron facility, the research team has also developed the flow chart in Figure 38 for ROV stability analysis, which uses a robust Proportional-Integral-Derivative (PID) control.

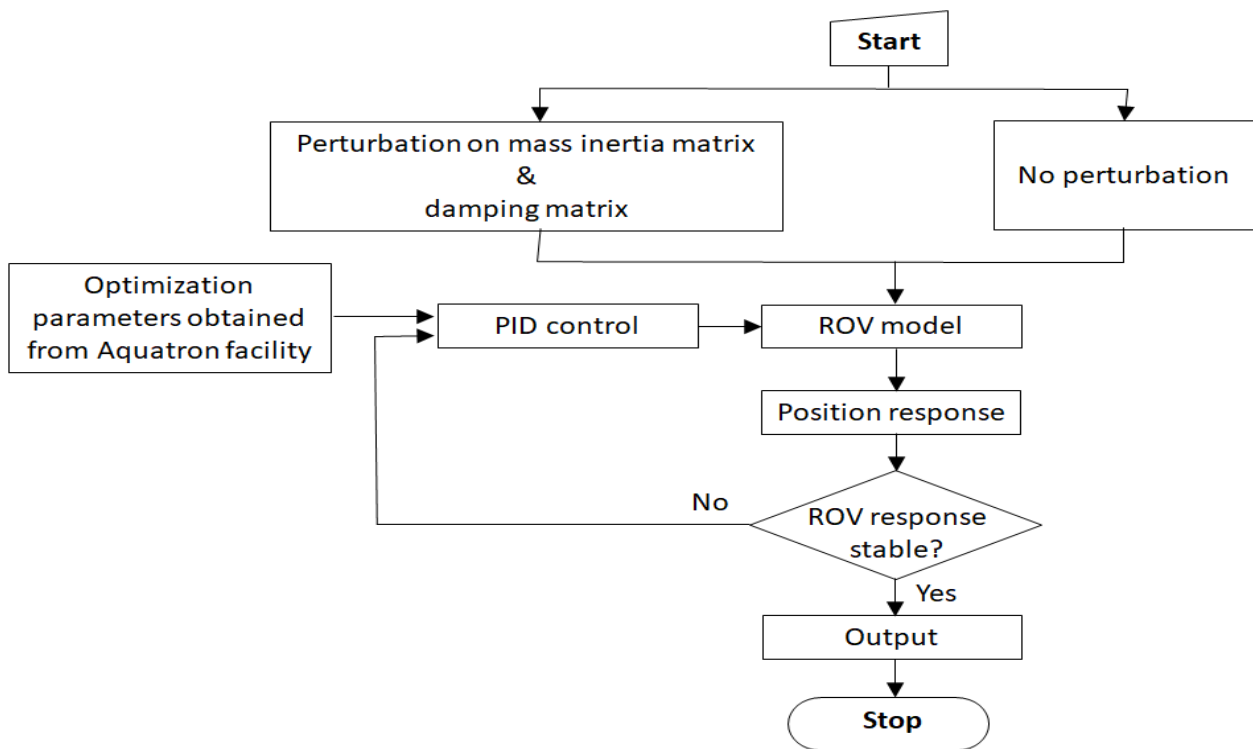


Figure 38: Flow chart of the PID control optimization.

To test the robustness of this PID control, the ROV's mass inertia and diagonal hydrodynamic damping matrix were allowed to vary within a limit specified by the proposed optimized design. These variations derive from possible change in the mass distribution in the ROV. The limits are obtained using a CAD software such as SolidWorks or Autodesk Inventor. By changing the mass properties of each targeted component, a different mass inertia matrix is obtained. The limits are determined by evaluating the differences between the nominal and new mass inertia matrix. The PID control parameters are obtained from the simulations output response. This helps establish further optimization requirements of the ROV.

VI-2- Proposed activities for tank testing

Following DDL's withdrawal from the project (only three weeks before the scheduled testing) and unavailability of the Cougar ROV, the research team had to update simulation results using the Seaeye Falcon 12423 ROV. As this is a time computationally demanding task, we have limited ourselves to scenarios achievable during the one-week available time-window for testing in the Aquatron facility. The following activities were therefore planned and simulated prior to pool tank testing.

- **Trial 1: ROV only**

→ Holding station on bottom: the ROV is deployed at the bottom of the Aquatron and held in position, at 0° heading. The flow rate is gradually increased from 50% to 100% of full tank capacity (based on four pumps) with a step increment of 10%. Each flow rate is maintained a few minutes to enable data collection. During this time, power consumption is collected from the ROV main operation station. This scenario is replicated for 90° heading. All thrusters' power consumptions are collected accordingly, from which the reaction loads are calculated and correlated with the simulation results in Figures 39 to 44 below:

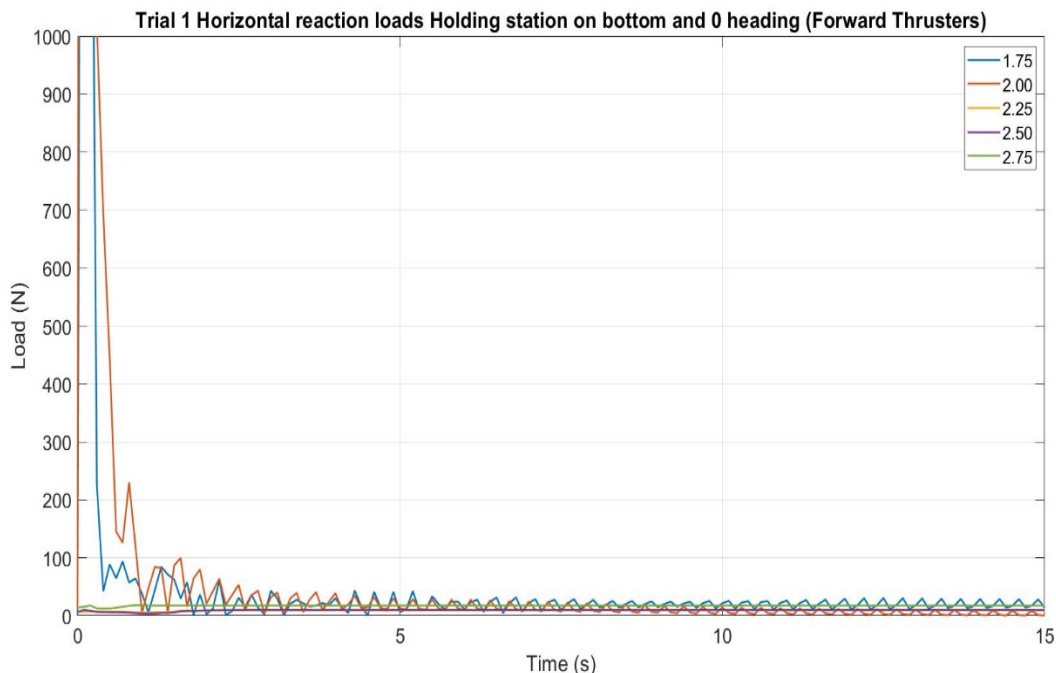


Figure 39: Horizontal reaction loads – Holding station on bottom and 0° heading (Forward thrust).

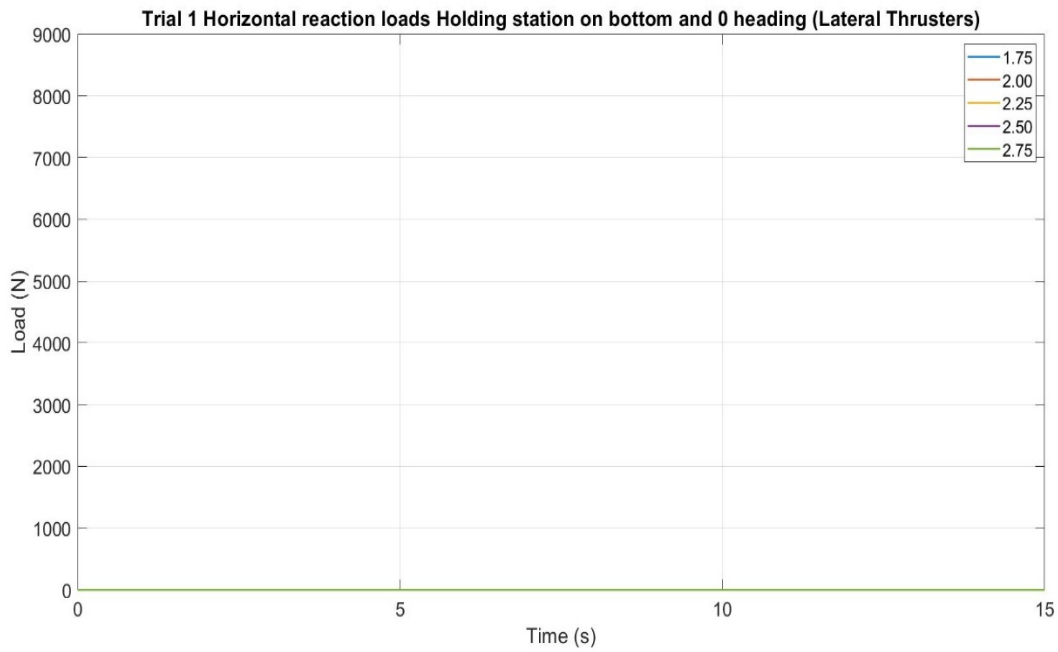


Figure 40: Horizontal reaction loads – Holding station on bottom and 0 heading (Lateral thrust).

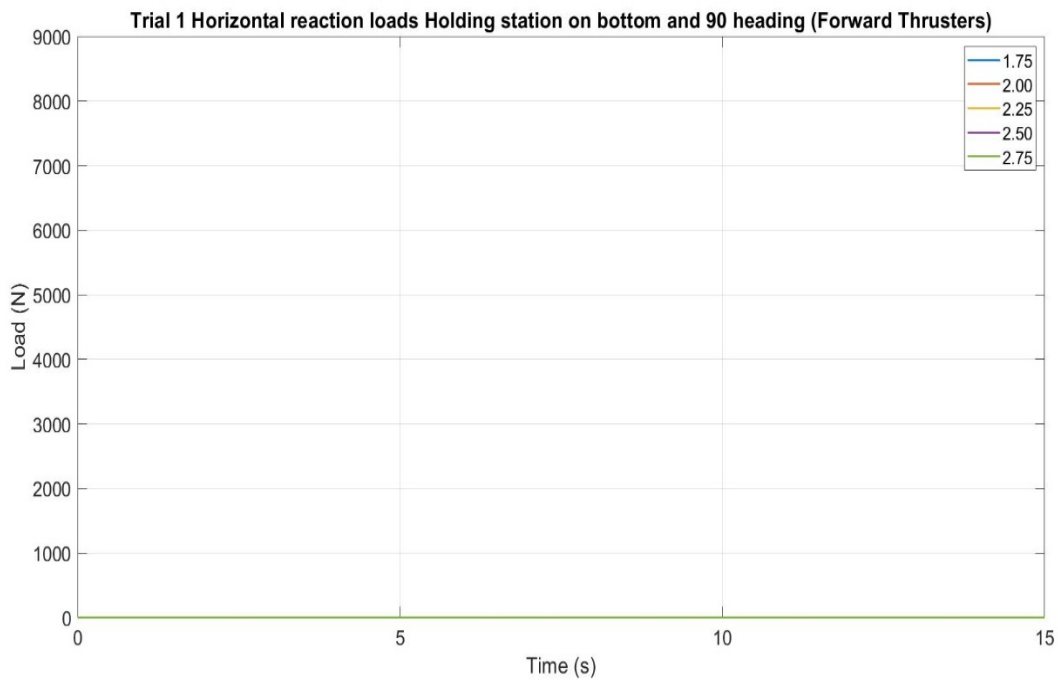


Figure 41: Horizontal reaction loads – Holding station on bottom and 90 heading (Forward thrust).

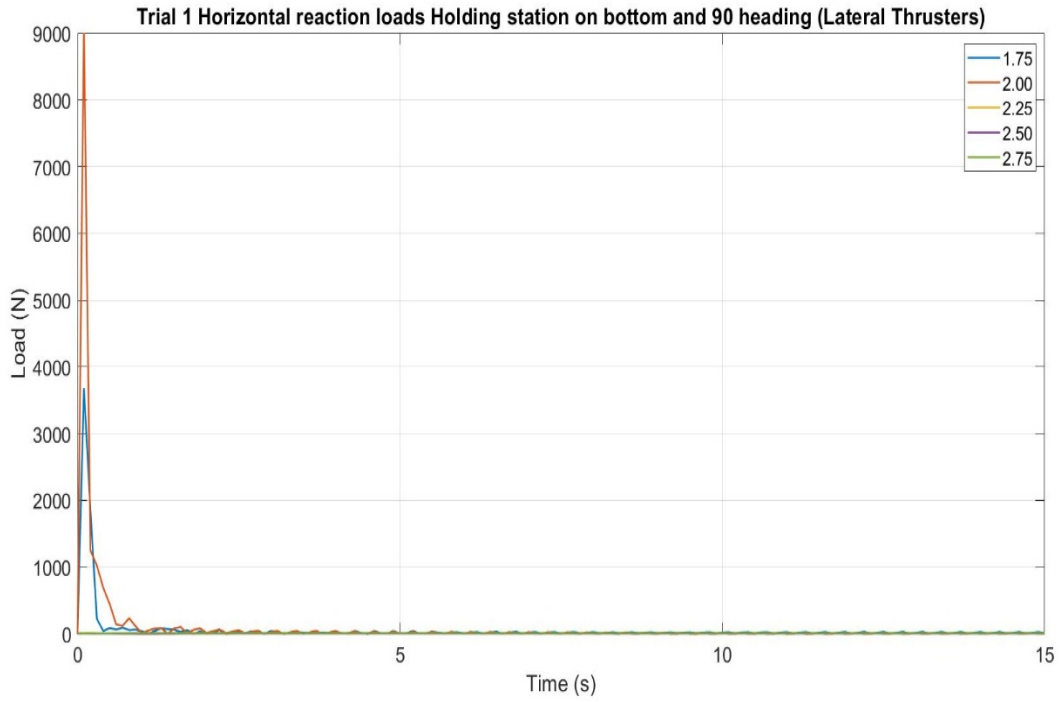


Figure 42: Horizontal reaction loads – Holding station on bottom and 90 heading (Lateral thrust).

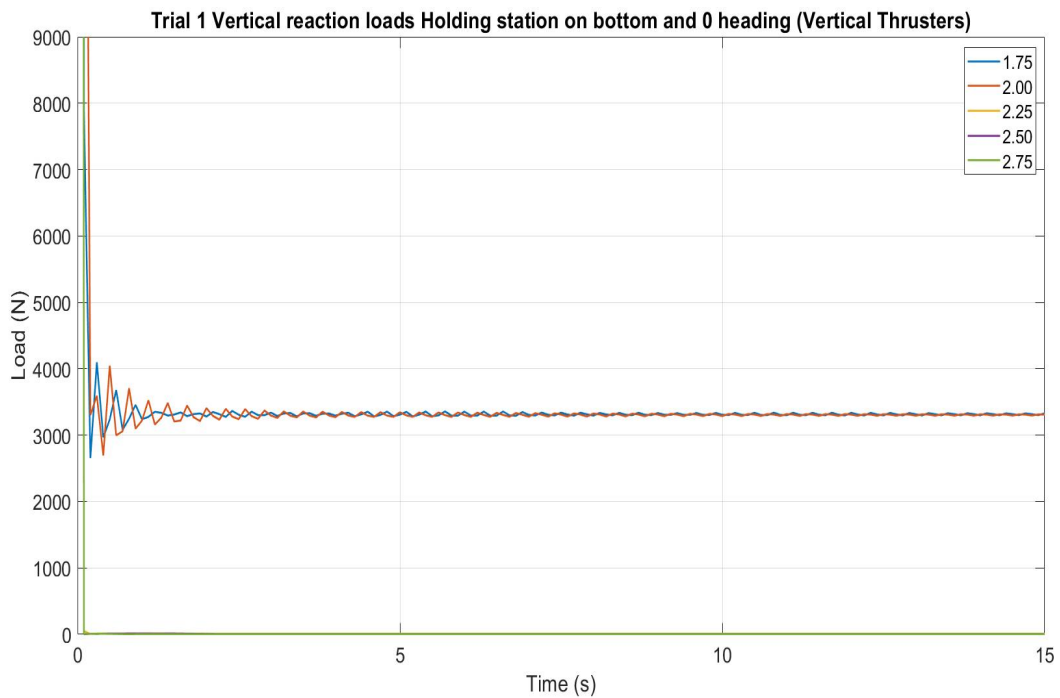


Figure 43: Vertical reaction loads – Holding station on bottom and 0 heading (Vertical thrust).

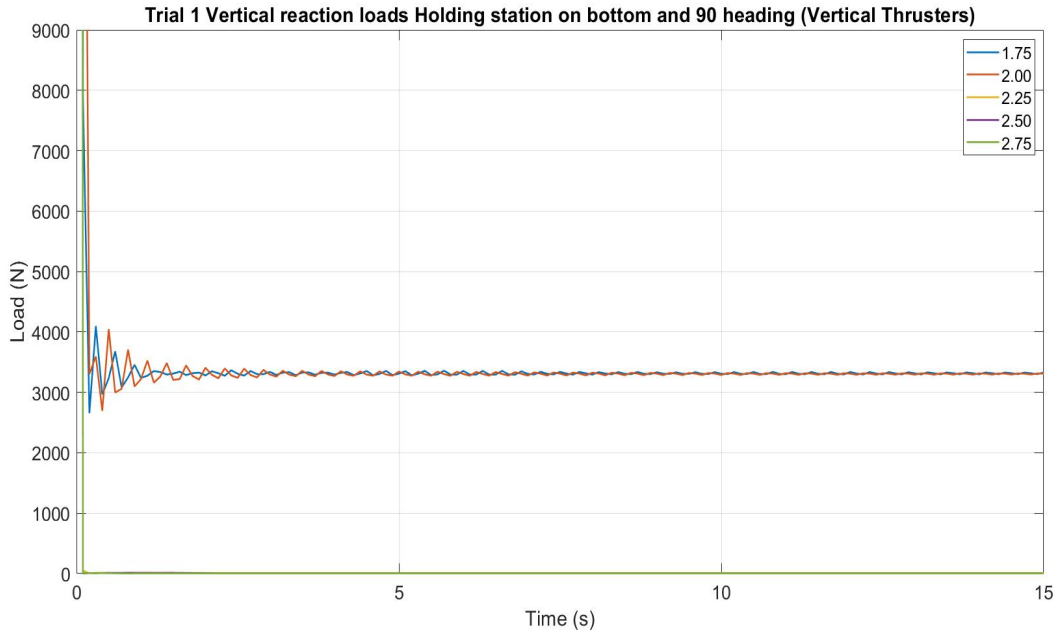


Figure 44: Vertical reaction loads – Holding station on bottom and 90 heading (Vertical thrust).

→ Holding 1m above Aquatron bottom: the ROV is deployed at 1m above the bottom of the Aquatron and held in position, at 0° heading. The flow rate is then gradually increased from 50% to 100% with a step increment of 10%. Each flow rate is maintained a few minutes to enable data collection. During this time, power consumption is collected from the ROV main operation station. This scenario is replicated for 90° heading. All thrusters' power consumptions are collected accordingly, from which the reaction loads are calculated and correlated with the simulation results in Figures 45 to 50 below:

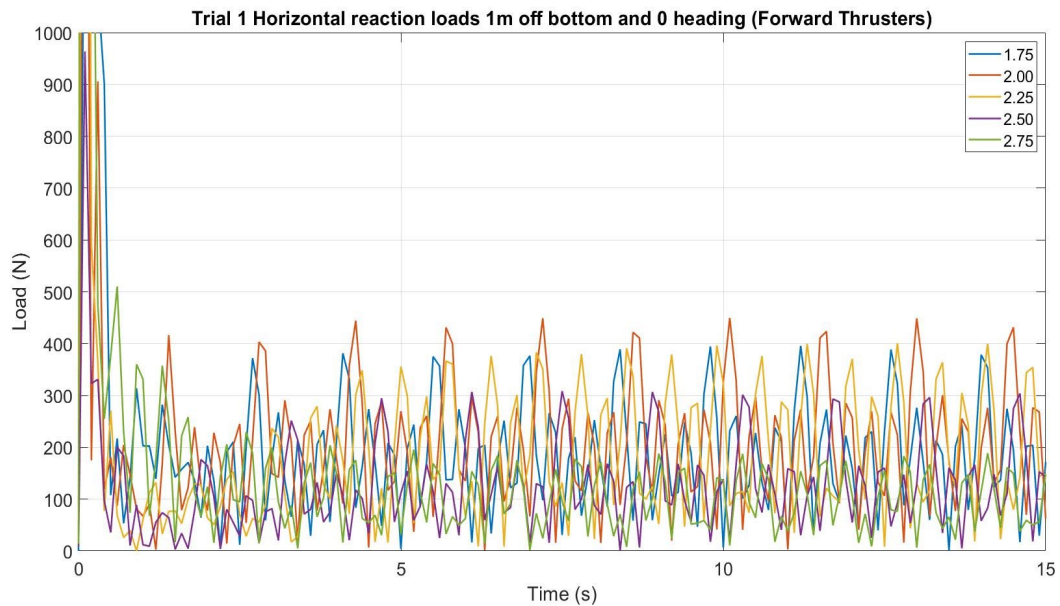


Figure 45: Horizontal reaction loads – 1m off bottom and 0 heading (Forward thrust).

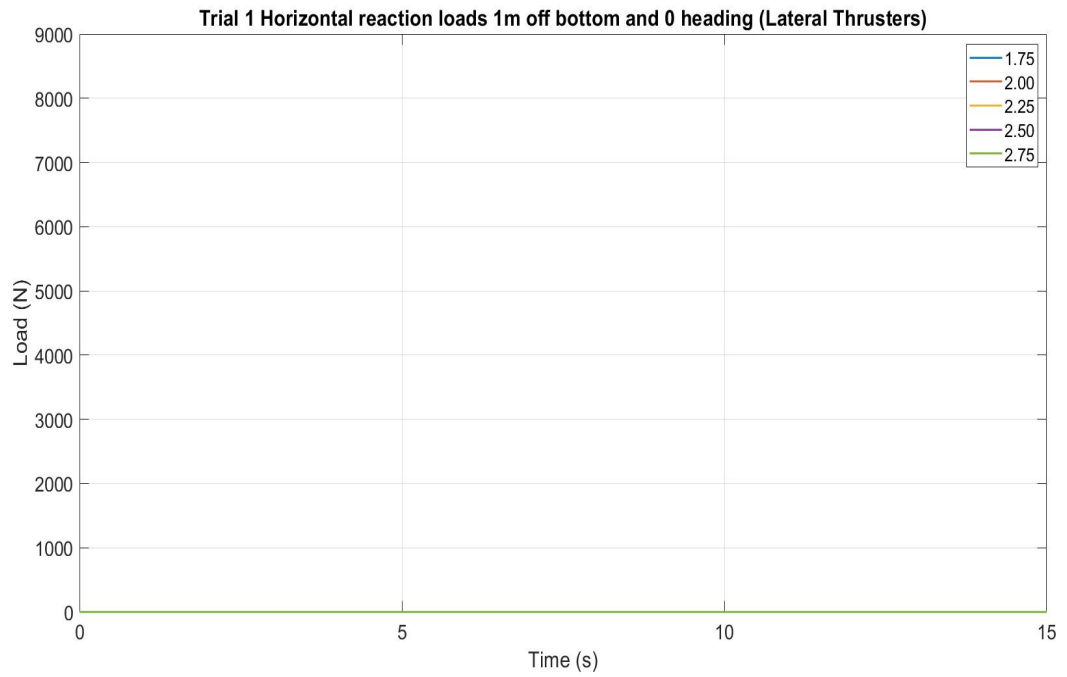


Figure 46: Horizontal reaction loads – 1m off bottom and 0 heading (Lateral thrust).

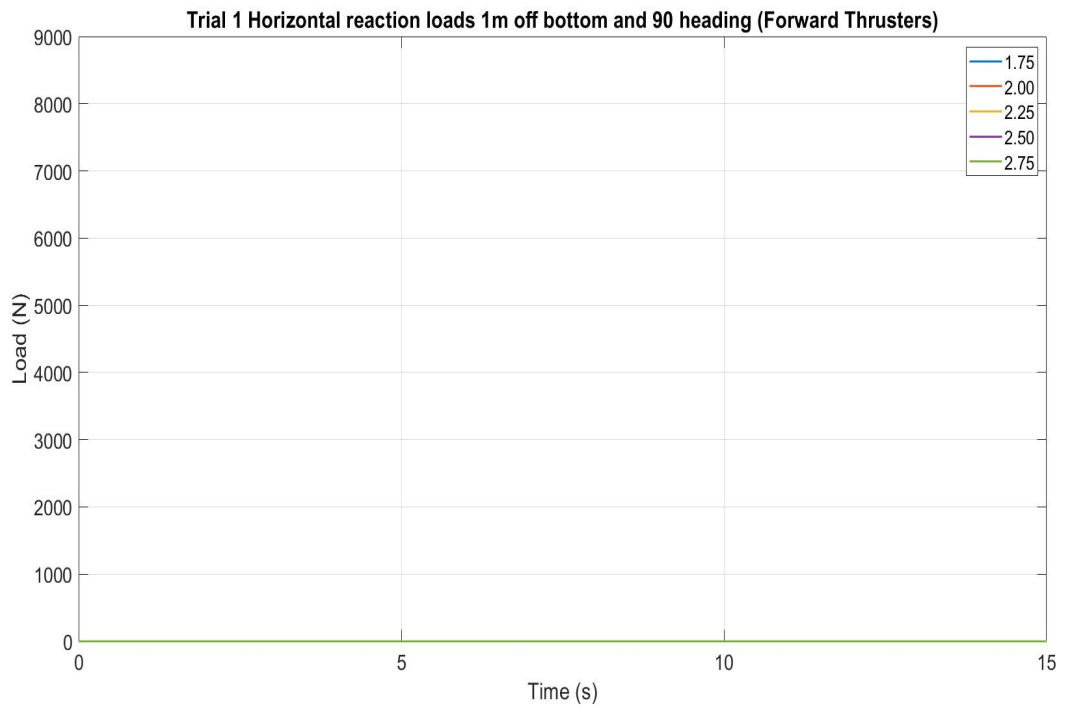


Figure 47: Horizontal reaction loads – 1m off bottom and 90 heading (Forward thrust).

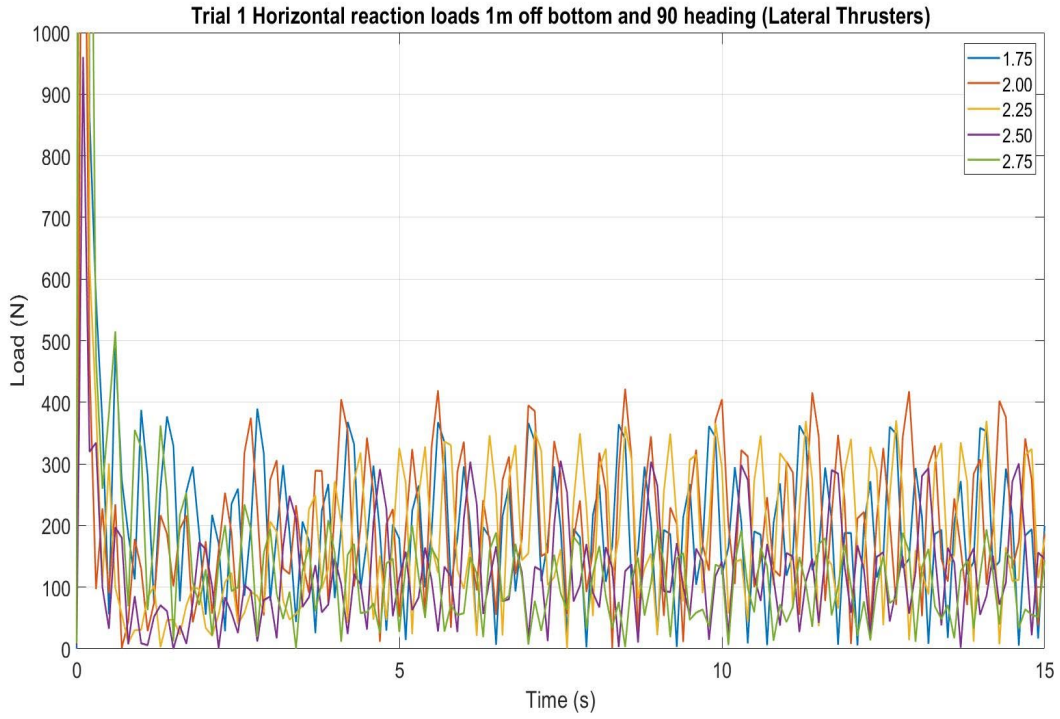


Figure 48: Horizontal reaction loads – 1m off bottom and 90 heading (Lateral thrust).

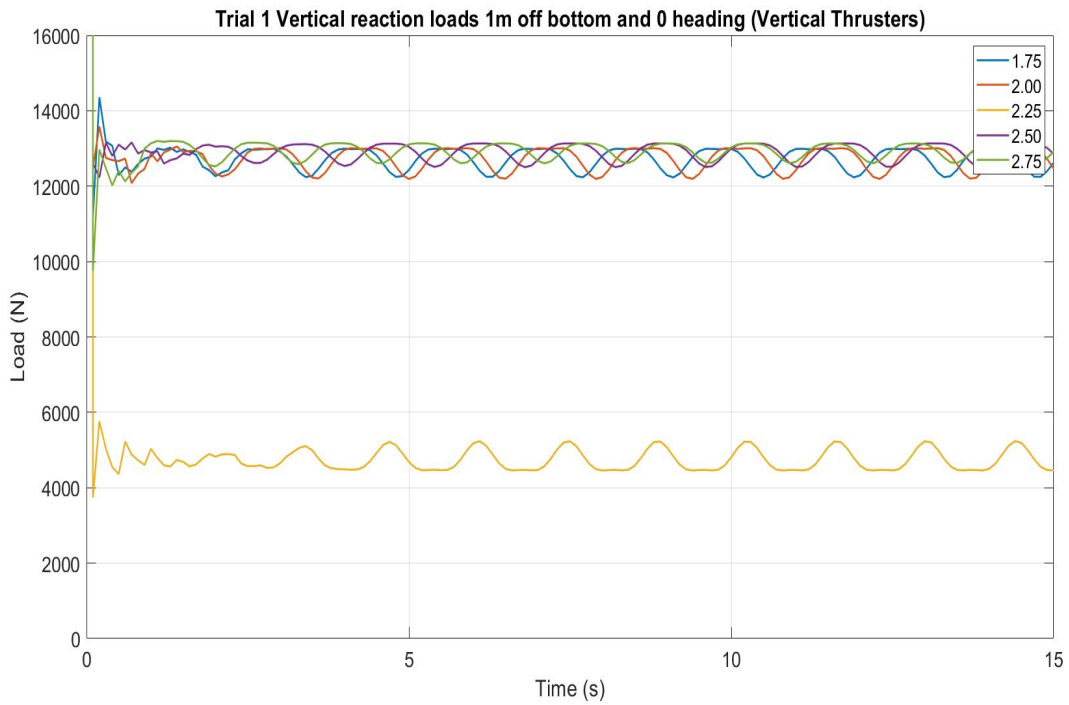


Figure 49: Vertical reaction loads – 1m off bottom and 0 heading (Vertical thrust).

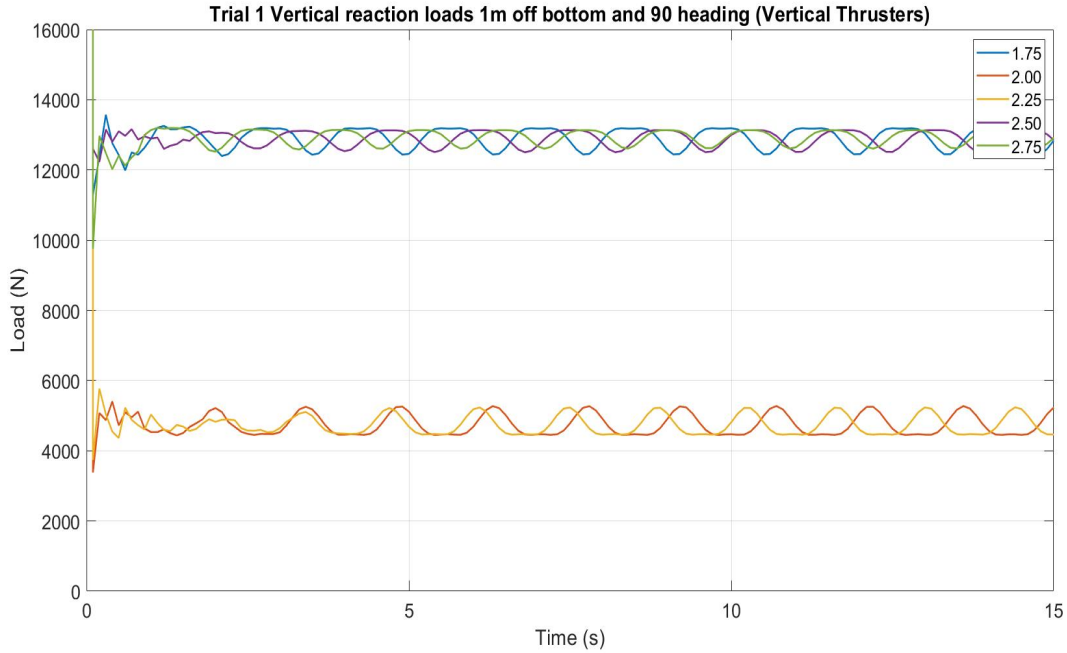


Figure 50: Vertical reaction loads – 1m off bottom and 90 heading (Vertical thrust).

- **Trial 2: ROV & Dual-arm skids**

→ In these experiments, the dual-arm skid is mounted onto the ROV and all the above procedures for Trial 1 are repeated and will be correlated with the simulated results in Figures 51 to 58 below:

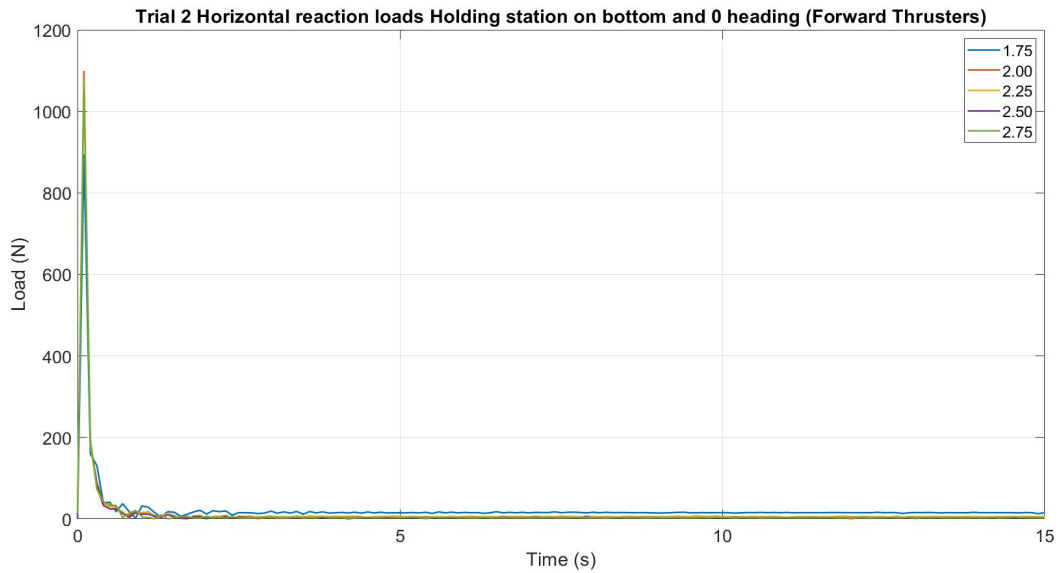


Figure 51: Horizontal reaction loads – Holding station on bottom and 0 heading (Forward thrust).

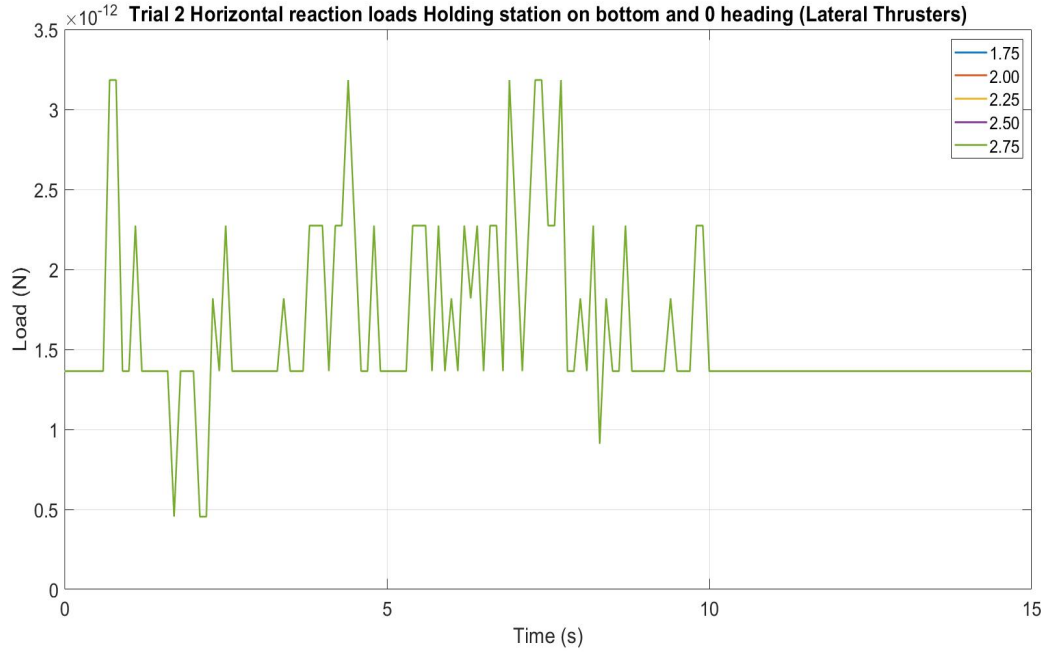


Figure 52: Horizontal reaction loads – Holding station on bottom and 0 heading (Lateral thrust).

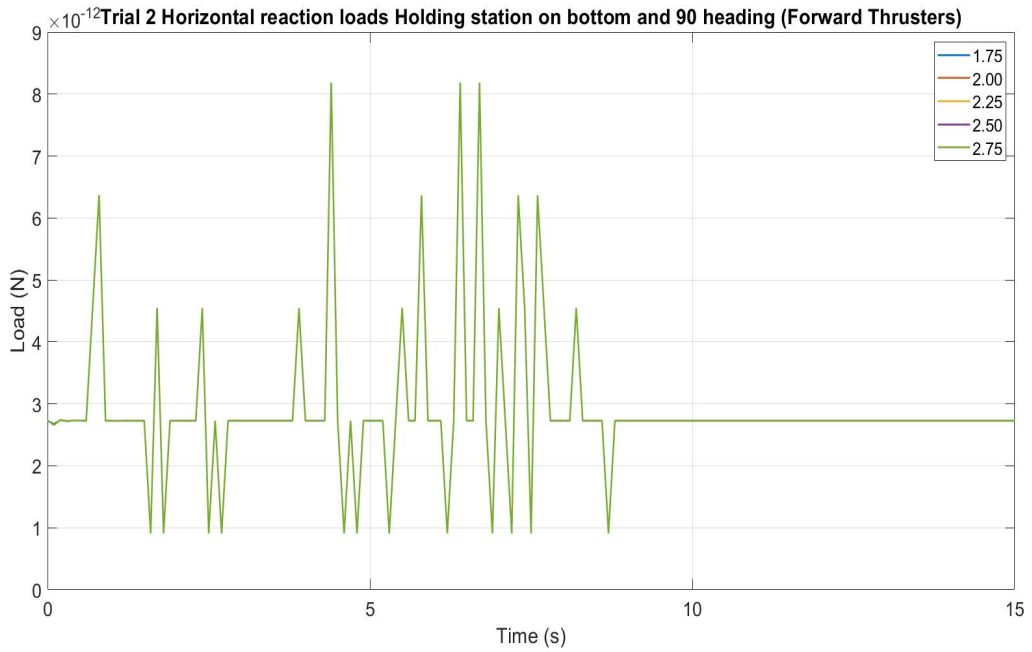


Figure 53: Horizontal reaction loads – Holding station on bottom and 90 heading (Forward thrust).

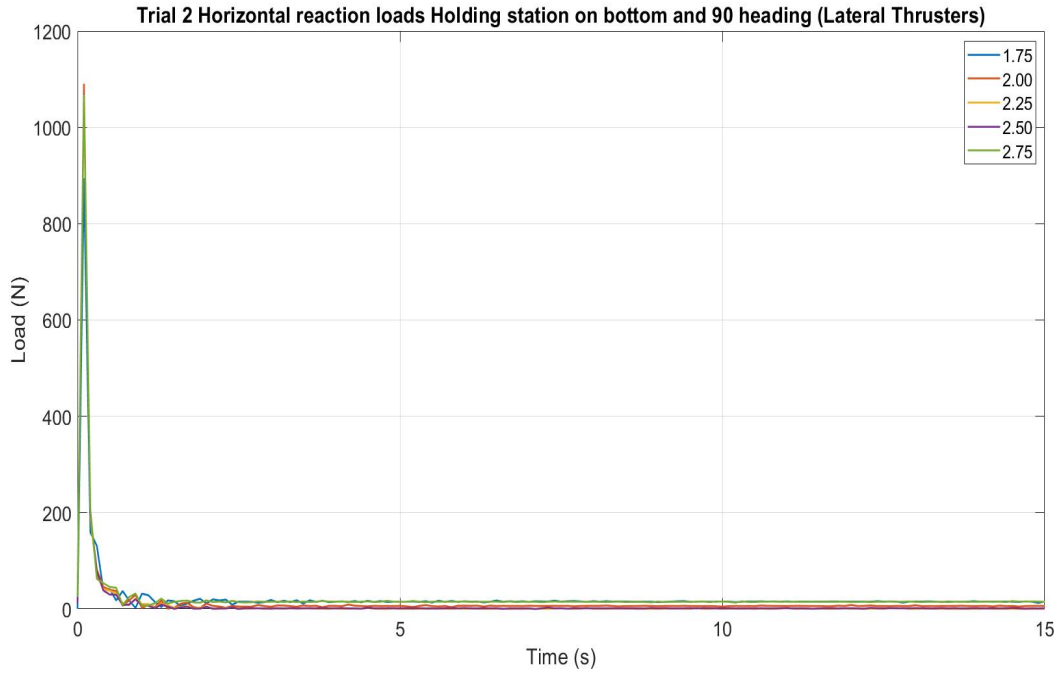


Figure 54: Horizontal reaction loads – Holding station on bottom and 90 heading (Lateral thrust).

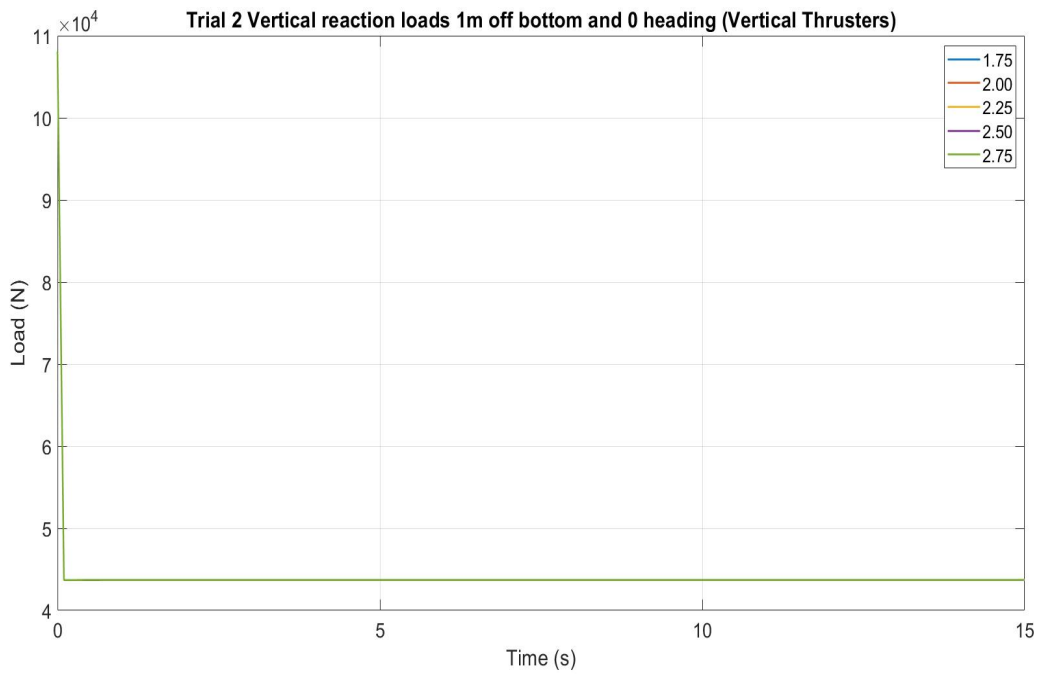


Figure 55: Vertical reaction loads – 1m off bottom and 0 heading (Vertical thrust).

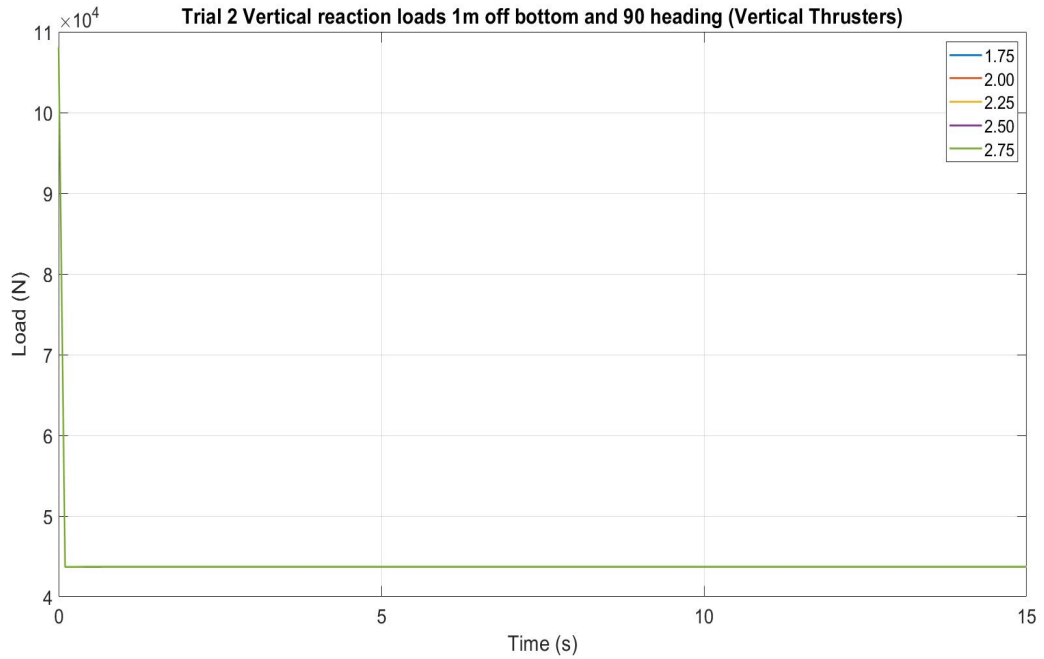


Figure 56: Vertical reaction loads – 1m off bottom and 90 heading (Vertical thrust).

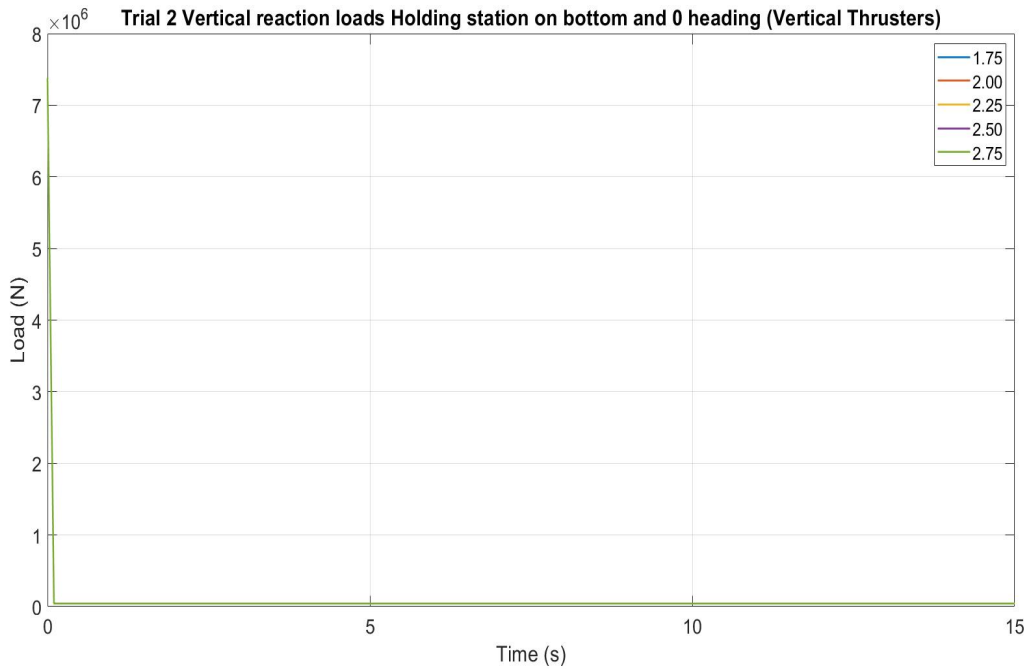


Figure 57: Vertical reaction loads – Holding station on bottom and 0 heading (Vertical thrust).

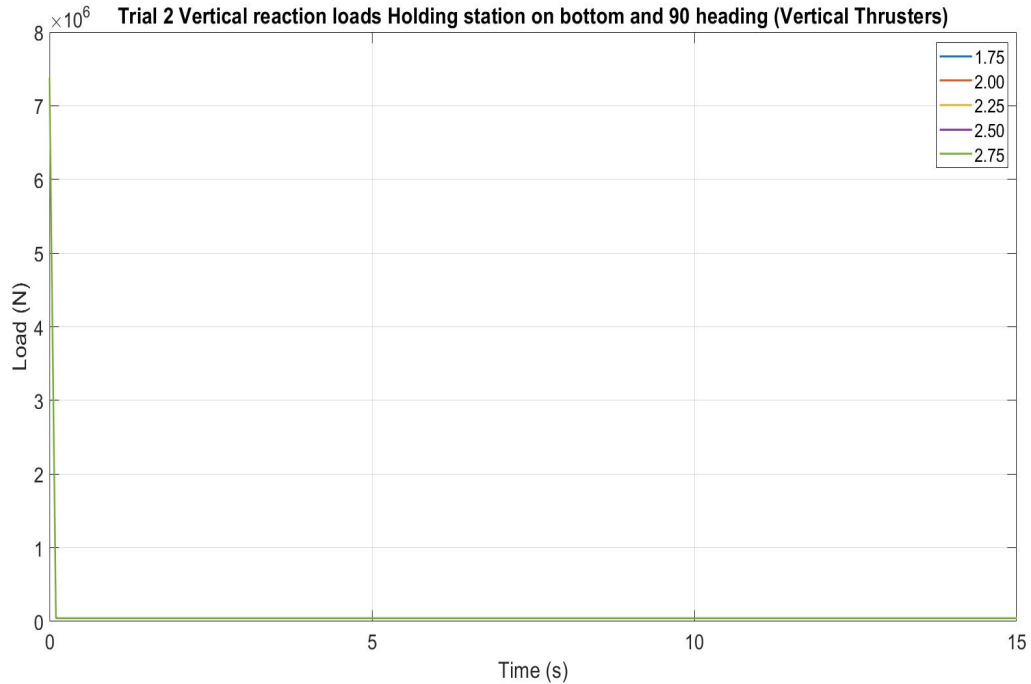


Figure 58: Vertical reaction loads – Holding station on bottom and 90 heading (Vertical thrust).

- **Armored vs normal umbilical**

The research team has planned to swap the umbilical on the ROV and Trial 1 and 2 above then repeat the experiments with an armored umbilical, with the objective to compare experimental results with numerical simulation from ProteusDS and ShipMo3D. Simulation parameters were adjusted accordingly and the whole simulation process repeated. This iterative process was to be conducted until satisfactory simulation parameters are obtained. Unfortunately, the unavailability of an armored umbilical has stopped this initiative.

VII- MODELING CAPABILITIES IMPROVEMENT EFFORTS

VII-1- Estimating hydrodynamic parameters of the ROV

Scope

This section addresses the feasibility of estimating hydrodynamic parameters of the ROV such as added mass and damping coefficients. These parameters affect the ROV's acceleration and maneuverability. These parameters affect the ROV's acceleration and maneuverability and estimating them in yaw, surge, sway and heave are required to develop 6 degrees of freedom time-domain numerical model of the ROV. The added mass is commonly considered a hydrodynamic parameter usually obtained through expensive tank tests where the ROV is subjected to oscillations. This is commonly conducted using WAMIT³, the most advanced set of tools available

³ Chin, C.S., Lin, W.P. & Lin, J.Y. Experimental validation of open-frame ROV model for virtual reality simulation and control. Journal of Marine Science and Technology, pp 1-21 (2017). <https://doi.org/10.1007/s00773-017-0469-3>.

for analyzing wave interactions with offshore platforms and other structures or vessels. This product is not available at an affordable cost and the current project will investigate the feasibility of using other products such as ShipMo3D⁴ or NEMOH⁵ for the determination of added mass at infinite frequency. The project has also evaluated the rotational damping coefficients obtained from the potential flow theory⁶, which are difficult to obtain through Computational Fluid Dynamics (CFD).

Numerical configuration and simulation

In using ShipMo3D, the sizes of the cuboids are those from ROV configurations *Trial 1* and *Trial 2*. This was done so the results from ShipMo3D can directly be imported into the ProteusDS to complement the previous simulations. The configurations were as follows;

Trial 1: ROV only - Normal Umbilical

- Holding station on the bottom
- Holding station approximately 10 m off the bottom
- Mimic flying straight line surveying seabed

Trial 2: ROV and Dual-Arm Skid - Normal Umbilical

- Holding station on the bottom
- Holding station approximately 10 m off the bottom
- Mimic flying straight line surveying seabed

The Cuboid CAD drawings were created in Inventor Professional 2019. They were then imported to Altair Hypermesh for meshing and were exported to .obj file format (compatible with ShipMo3D). Tables 1 and 2 below show the dimensions of the cuboid used for Trial 1 and Trial 2 respectively.

Table 1: ROV cuboid dimensions

ROV only Cuboid	
X	0.914 m
Y	0.712 m
Z	1.336 m

⁴ McTaggart, K.A. Verification and validation of ShipMo3D ship motion predictions in the time and frequency domains. *Int. Journal of Naval Architecture and Ocean Engineering* 3(1): 86-94, 2011.

⁵ Babarit, A., Delhommeau. Theoretical and numerical aspects of the open source BEM solver NEMOH. 11th European Wave and Tidal Energy Conference (EWTEC2015), Nantes, France, 2015,

⁶ Yu, Z., Shen, Y., Andahl, J., Breco, M. Implementation of Linear Potential-Flow Theory in the 6DOF Coupled Simulation of Ship Collision and Grounding Accidents. *Journal of ship research* 60(3), 119-144, 2016

Table 2: ROV and dual-arm skid cuboid dimension

ROV and dual-arm skid	
X	2.503 m
Y	0.695 m
Z	1.390

The mesh size was initially arbitrarily chosen and then refined after every simulation to the point where any decrease in mesh size did not produce a significant change in results. This optimal mesh size helped save time in each simulation. A picture of the meshed cuboid in Trials 1 and 2 can be seen in Figures 59 and 60 respectively.

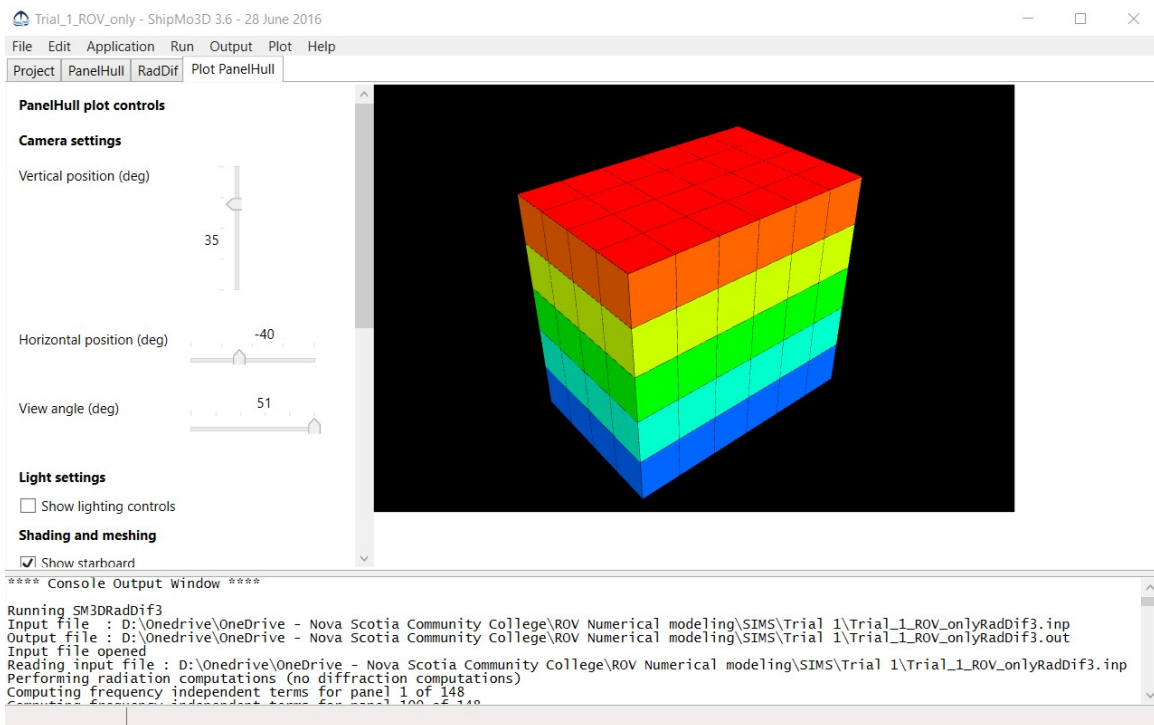


Figure 59: ROV only cuboid mesh for Trial 1.

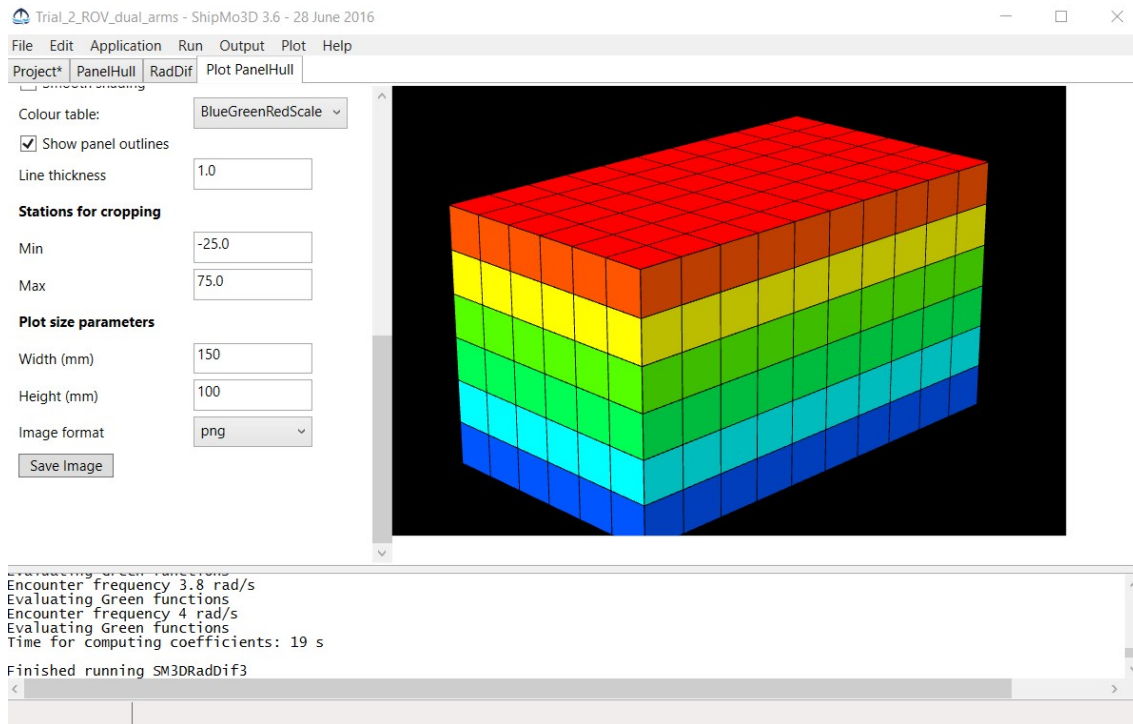


Figure 60: ROV and dual-arm skids cuboid mesh for Trial 2.

The cuboid was then placed with a draft of baseline at midship of 60 m and water density of 1025 kg/m^3 was also used. This depth represents the operating depth used for the DEMO project. The simulations all had the real-life parameters obtained from the Fundy Ocean Research Center for Energy (FORCE). The current speeds were set from 0 m/s to a maximum of 5 m/s. This range covers all the water currents encountered in the Bay of Fundy. The sea direction was always kept at 0° heading and the wave frequencies from 0.2 rad/s to 2 rad/s with increments of 0.1 rad/s. The cuboids were kinematically fixed in the ProteusDS simulation. This was adopted to mimic the ROV held in position and all the forces felt by the ROV calculated under that condition. These forces were then equated to the forces the ROV thrusters will need to exert in order to stay in position. Similarly, the cuboid was kept in fix position in the ShipMo3D simulation.

ShipMo3D simulation results

Figures 61, 62 and 63 show the results of the added mass and damping coefficients for the directions in longitudinal surge A11, Heave A33 and lateral pitch A55 for Trial 1. We observe that under kinematically fixed conditions, the damping coefficients are zero for all directions. They can therefore be ignored in Trial 1 configuration.

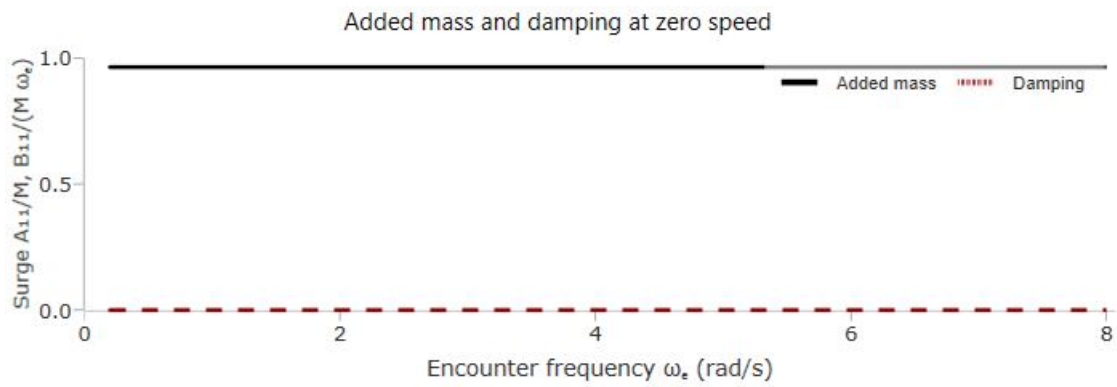


Figure 61: Surge Added mass and damping for Trial 1.

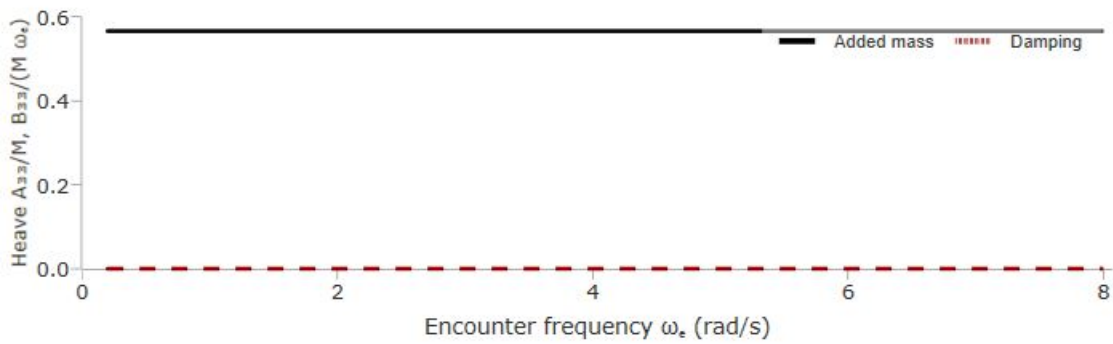


Figure 62: Heave added mass and damping for Trial 1.

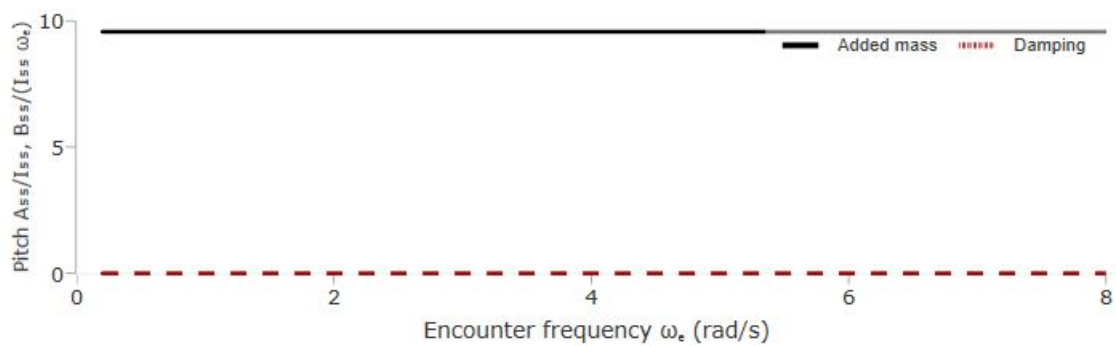


Figure63: Pitch added mass and damping for Trial 1.

Similarly, from figure 64, 65 and 66, we observe that the damping coefficients are also all 0 for all directions for Trial 2 configuration, and therefore can be ignored.

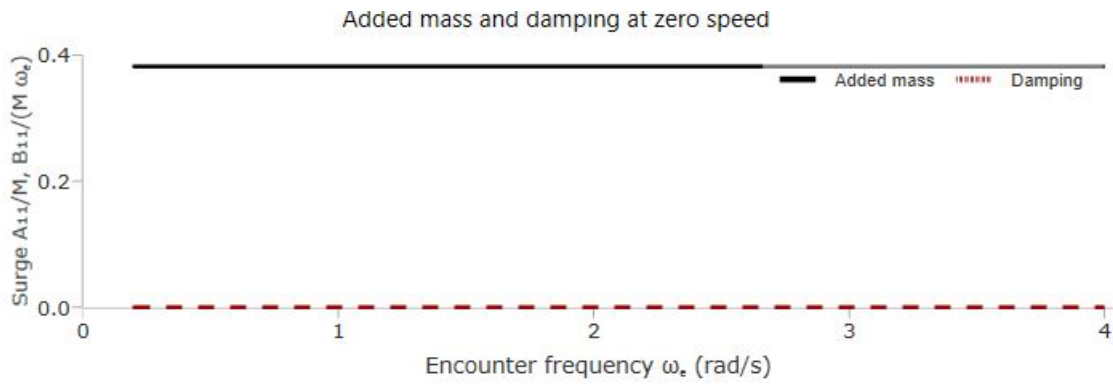


Figure 64: Surge added mass and damping for Trial 2.

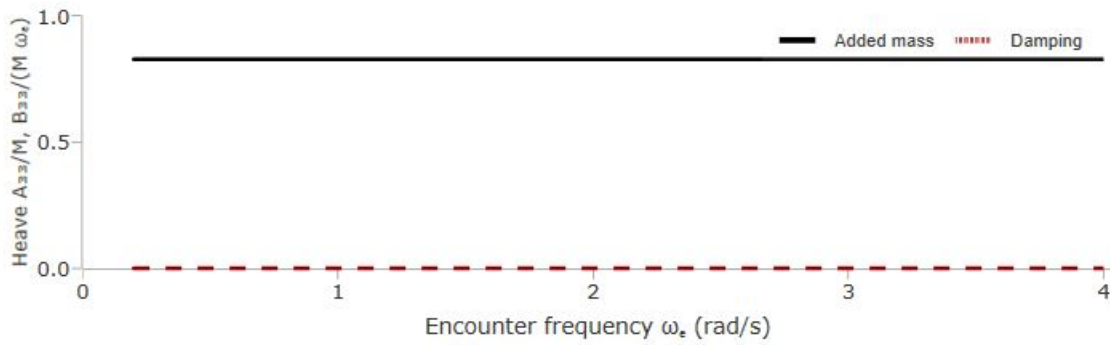


Figure 65: Heave added mass and damping for Trial 2.

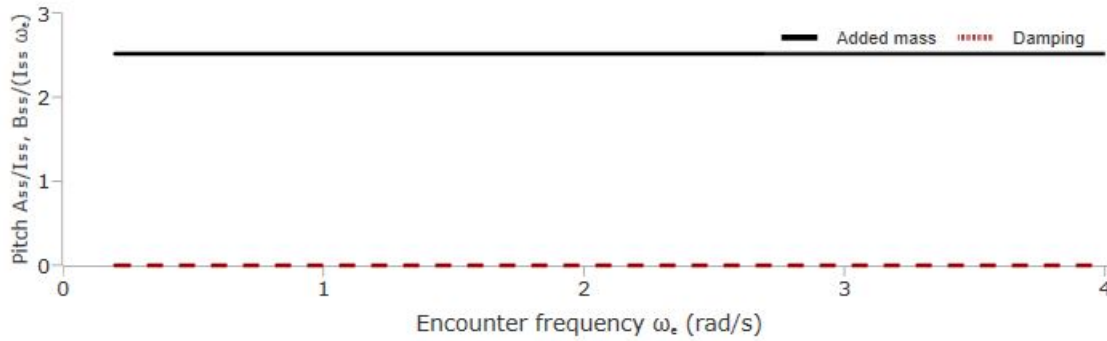


Figure 66: Pitch added mass and damping for Trial 2.

The ShipMo3D simulation results for Trial 1 and Trial 2 are summarized in Table 3 below:

Table 3: Summary of simulation results for Trial 1 and 2.

		Trial 1	Trial 2
Surge	$\frac{A_{11}}{M}$	1	0.4

	$\frac{B_{11}}{M\omega_e}$	0	0
Heave	$\frac{A_{33}}{M}$	0.6	0.7
	$\frac{B_{33}}{M\omega_e}$	0	0
Pitch	$\frac{A_{55}}{M}$	1	2.5
	$\frac{B_{55}}{I_{55}\omega_e}$	0	0

For a submerged body, fixed and far from the water surface, it is expected that the added mass and damping coefficients be negligible. The simulation results obtained agree with the expected values, the main reason being that the ROV cuboid was fixed in position. These results were then imported to the ProteusDS simulations for further validation in the Aquatron facility at Dalhousie University.

VII-2- Simulation-based optimization

As part of the scope of this DEMO project, Dr. Etienne Mfoumou and Mr. Jordan Kanga from NSCC had a one-week scientific visit at the University of Applied Sciences Upper Austria on February 11-15, 2019. Together with the team in Austria (Photo in Figure 67), we have developed an approach for applying their heuristic and evolutionary algorithms for optimizing data processing in the ProteusDS software. Simulation-based optimization was considered using Surrogate Modeling (SM), Machine Learning (ML), and Efficient Global Optimization (EGO).



Figure 67: NSCC research team posing with the research staff from Austria.

The simulation-based optimization from HEAL was required for the following reason:

- A **surrogate model** is an engineering method used when an outcome of interest cannot be easily directly measured, so a model of the outcome is used instead. Simulation optimization usually requires thousands or even millions of simulation evaluations to be completed, which was the case in this DEMO project.
- Each simulation can be very computationally demanding and expensive to compute making optimization not feasible (e.g 10 days 9 hours for some simulation configurations in the DEMO project, as illustrated in Figure 68 below).
- Surrogates replace expensive simulations by simple algebraic expressions fit to data.
- This approach is also used by Microsoft in its active malware services.

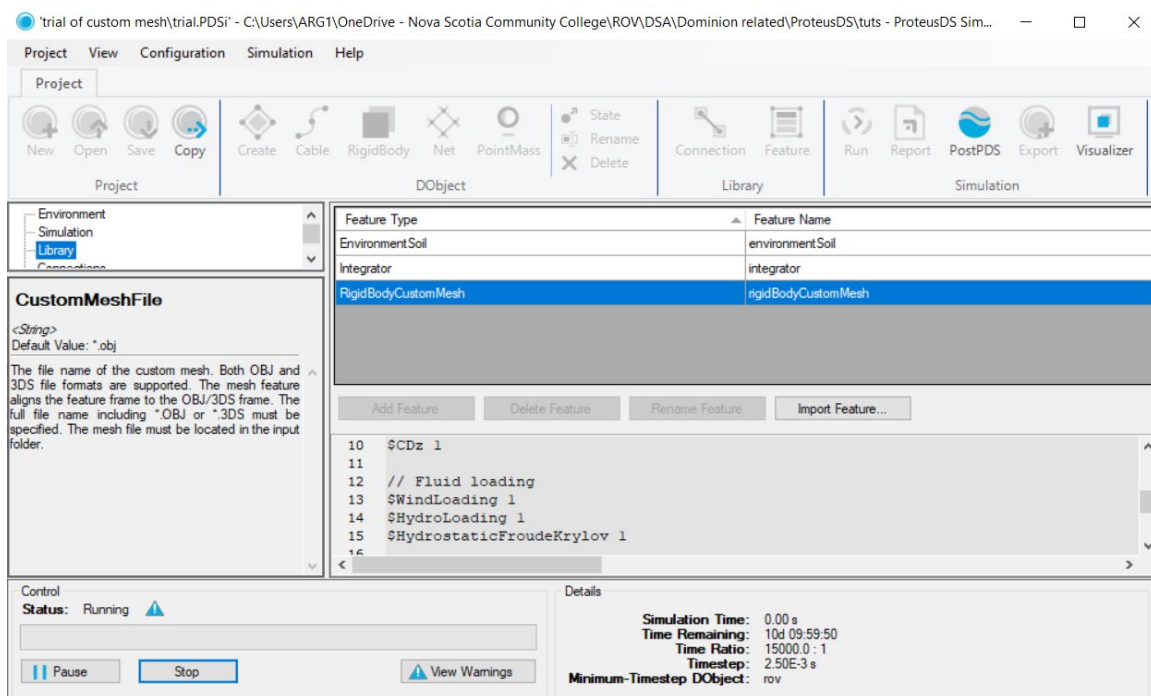


Figure 68: Computationally demanding simulation (10 days 9 hours) scenario justifying the need for optimization.

- **Machine learning** is an application of artificial **intelligence** (AI) that provides systems the ability to automatically learn and improve from experience without being explicitly programmed. Machine learning focuses on the development of computer programs that can access data and use it to learn for themselves. An example of display for a symbolic regression approach is shown in Figure 69 below.
- Machine learning was considered as an option for process optimization in the DEMO project because it enables the development of mathematical models to replace potential expensive simulation optimization tools.
- These models can be executed significantly faster compared to the actual ProteusDS simulation, which facilitates the processing of the intensive data available.

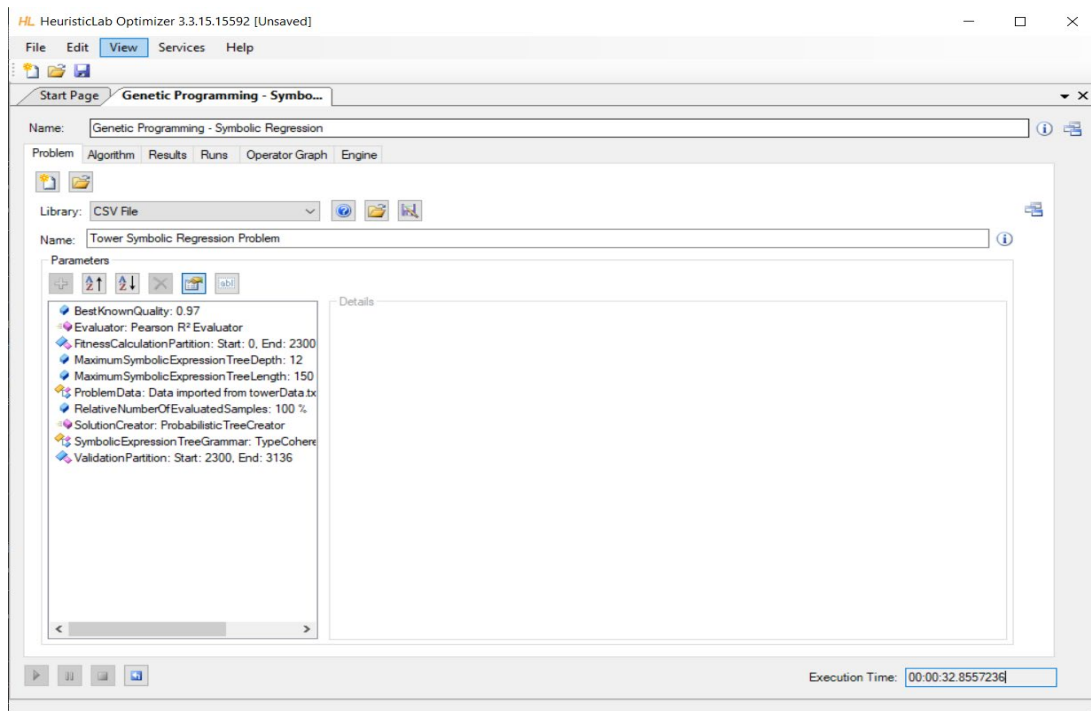


Figure 69: HeuristicLab Optimizer display for a Symbolic Regression problem.

- Efficient global optimization permits multidimensional surrogate modeling allowing the investigation of the effect of multiple inputs on a simulation model simultaneously, which is the case with data to be processed in the DEMO project.
- All code base software in C# language enables further iterations of the optimization process, as modeling capabilities specific requirements are expressed in the marine sector.

VIII- EXPERIMENTAL VALIDATION OF SIMULATED RESULTS

VIII-1- The Aquatron pool tank

The tank is made from reinforced concrete, with a glass reinforced polyester liner sealed with an epoxy coating. It is built atop a concrete tank stand with neoprene blocks sandwiched in between to partially acoustically uncouple the tank. The main deck is located at the top of the tank allowing access to all points of the tank surface (Figure 70).

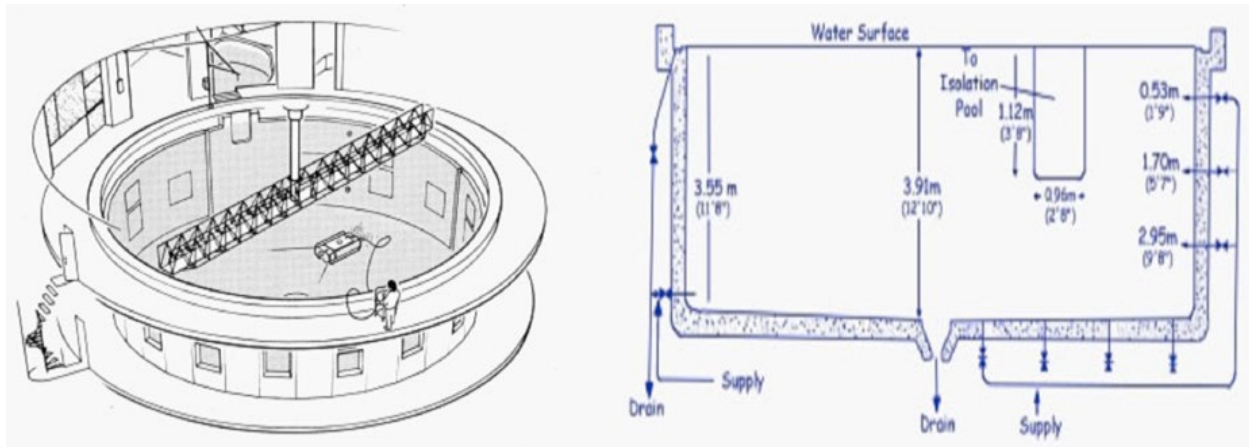


Figure 70: Diagrams of the pool tank showing the top view (left) and the side view with dimensions (right).

VIII-2- Description and features of the Falcon ROV

The SAAB Seaeye Falcon 12423 is a highly versatile Remotely Operated Vehicle (ROV) and can be employed to carry out a variety of survey, search, inspection and maintenance tasks (Figure 71). The operator or pilot uses a hand controller to ‘fly’ the ROV remotely by sending commands via an electrical umbilical. The ROV can be moved in any direction and by using its autopilot functions, can remain accurately on course and depth to provide a stable platform. The pilot can control the vehicle’s video system, lighting and all other equipment fitted.

During the DEMO experiments, “auto-depth” function was used to ensure the ROV is within the jet outlet level throughout the experiments, for testing with the ROV off the bottom tank. A standard partition of the PC SSD is provided for saving data and video recordings or snapshots. The front camera was mainly used to visualize the location of the ROV relative to the jet outlet. The Falcon System also incorporates a touchscreen monitor that displays the video information from the camera and system information as widgets (or docking panels) around the perimeter (Figure 72).



Figure 71: SAAB SeaEye Falcon 12423 (left), hand control unit (middle), and power supply unit front control panel with digital voltage and current display.



Figure 72: SAAB SeaEye Falcon 12423 touchscreen monitor displaying the video information from the camera and system information as widgets.

The thrusters are a very crucial component of the ROV determining the current magnitude the ROV could operate within before being overthrown. Each Thruster provides 13 kgf (at 240W Power) of propulsive thrust. Four thrusters control horizontal movement and one controls vertical ascent and descent. (Figures 73 & 74). The horizontal thrusters are angled at 35° from the ROV longitudinal axis providing a higher forward and backward thrust during operation.



Figure 73: Horizontal (left), and vertical (right) thrusters.



Figure 74: Schematic top view of ROV thrusters (left), Thrusters mounting position and angle with all thrusters idle (middle), and Thruster at 60% in a clockwise direction (right).

The Navigation Pod contains a solid-state magnetoresistive compass, a MEMS gyroscope, and a depth transducer. Depth, Pitch & Roll and heading signals from these components are displayed on the monitor as well as being combined internally to provide the Falcon ROV with its Auto functions, which adjusts the thrusters to maintain depth and heading. The head-on ROV configuration (90°) on the magnetoresistive compass was determined visually when observing the jet outlet using the front camera, while the transverse configuration (180°) orientation was determined to be 90° from the head-on orientation.

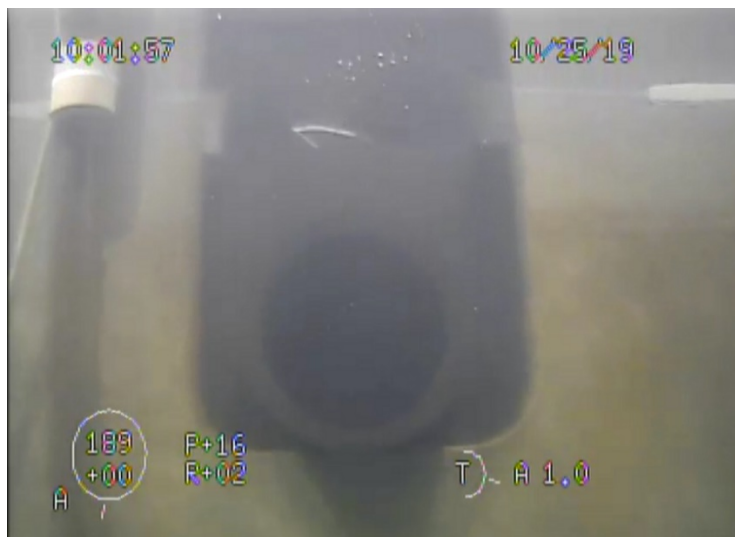


Figure 75: Head-on ROV configuration, determined by observing jet outlet using the front camera

The high amount of steel in the Aquatron Pool Tank structure interfered with the ROV compass magnetically during the experiments, affecting the accuracy of the ROV orientation measurements. Large discrepancies were observed and adjusted visually, however error is unavoidable.

The Falcon is fitted with the gyro-stabilised, multi-frequency sonar, which provides high resolution scans with reduced blurring. This was used to determine the location of the ROV relative to the Aquatron Pool Tank wall. Although the sonar accuracy of measurement is high, the ability

of the ROV operator to stabilize the ROV in position (especially at high currents) is limited, resulting in certain fluctuations in location and all other measurements as well.

VIII-3- Experimental Procedure

Two set of experiments were performed using the ROV in the Aquatron Pool Tank. Experiment (1) included the Ballast Skid fixed on the ROV, while Experiment (2) had the ROV only, with no skid. The manipulator arm was not included in either experiments. All experiments were performed while the ROV is at the jet outlet water level and along its axis. This is to experience the effect of flow on the ROV since the Aquatron Pool Tank considerably dampens the flow due to the large stagnant volume of water it contains.

Experiment (1) – ROV + Ballast Skid:

To determine the threshold the ROV could manage, the ROV is located at the jet outlet and a single pump is run at 40% of its power (40% is the minimum power each pump could be run). The operator maintains the ROV location in position and videos recordings are taken for the display monitor (displaying camera front video, compass angle, roll, pitch and the percentage of power consumed by the five thrusters), the power supply unit front control panel (displaying live total voltage and current during operation). The conditions of each configuration are recorded separately including the ROV location, pump power percentage, location using sonar, and date and time. This was performed to track the results extracted from the different devices for data processing. The ROV is kept in position in front of the jet outlet and the pump power is increased gradually by increments of 10% until 100%. A waiting time of 2-3min after each increment is adopted to ensure that the flow in the Aquatron Pool Tank reached a steady state flow condition. An additional pump is then run increasing its pump power percentage from 40% to 100% as well. However, it was not possible for the ROV operator to hold the ROV in position when the second pump was run. Therefore, measurements were taken while the ROV was at different locations along the jet axis ranging from the end (opposite to the jet outlet) to the center of the tank (~12m to ~7m). The increments were approximately 1m while the actual numbers are in the results section. When the second pump was at 90% while the first was at 100%, the ROV operator was finding it not possible to stabilize the ROV at its location and prevent ROV spinning as we reached the center of the tank (~7m). Therefore, the measurements taken while the second pump was running at 90% and 100% are not reliable.

Experiment (2) – ROV Only:

Here the Ballast Skid is removed from the ROV. The ROV limit is predicted from Experiment (1). Therefore, measurements were taken as the percentage of pump power increased incrementally from 40% to 100% for the first pump, while ROV is positioned at the tank center (~7m) and moved in increments of approximately 1.5m until the jet outlet is reached. The ROV operator managed to sustain the position of the ROV at the designated locations until the additional second pump power reached 50%. While running the additional pump at 60 and 70%, measurements were taken from the end to the center of the tank (~12m to ~7m). At 80% of the additional second pump running, the ROV operator was facing difficulties holding the ROV in position and the actual depth of the ROV was 1.5m (rather than 0.7 – 0.8m) although the vertical thruster was running at its maximum capacity. This is a result of the “coned” downward water

flow pushing from the top of the ROV. At 90 and 100% of the additional second pump power, it was only possible to take measurements at the end of the tank (~12m).

VIII-4- Data processing

Video recordings of the whole experiments were transferred from the Falcon System. However, the live measurements of current, voltage, and thruster power consumption percentages performed by the Falcon System are displayed but not recorded by the system. Therefore, short video recordings of the different screens were performed using external cameras to extract the required data for further processing.

The first step in analyzing data was to import them into MATLAB workspace. A structure array-type data organization was adopted, as it groups data, for each water flow rate, using data containers called fields. The fields were defined as:

- Location of the ROV in the tank: distance from the jet outlet;
- Depth: distance from the ROV's location to the water surface;
- Vertical: total vertical thrust;
- FR%: percentage right forward thrust with respect to thruster's full capacity;
- FL%: percentage left forward thrust with respect to thruster's full capacity;
- BR%: percentage right back thrust with respect to thruster's full capacity;
- BL%: percentage left back thrust with respect to thruster's full capacity;
- Volt: voltage consumed by the ROV;
- Amp: amperage consumed by the ROV;
- Forward: total forward thrust; and
- Lateral: total lateral thrust.

VIII-5- Results and interpretation

ROV only (no skid)

A 3D plot of the Forward Total Thrust at each flow rate along the jet axis is shown in Figure 76 below.

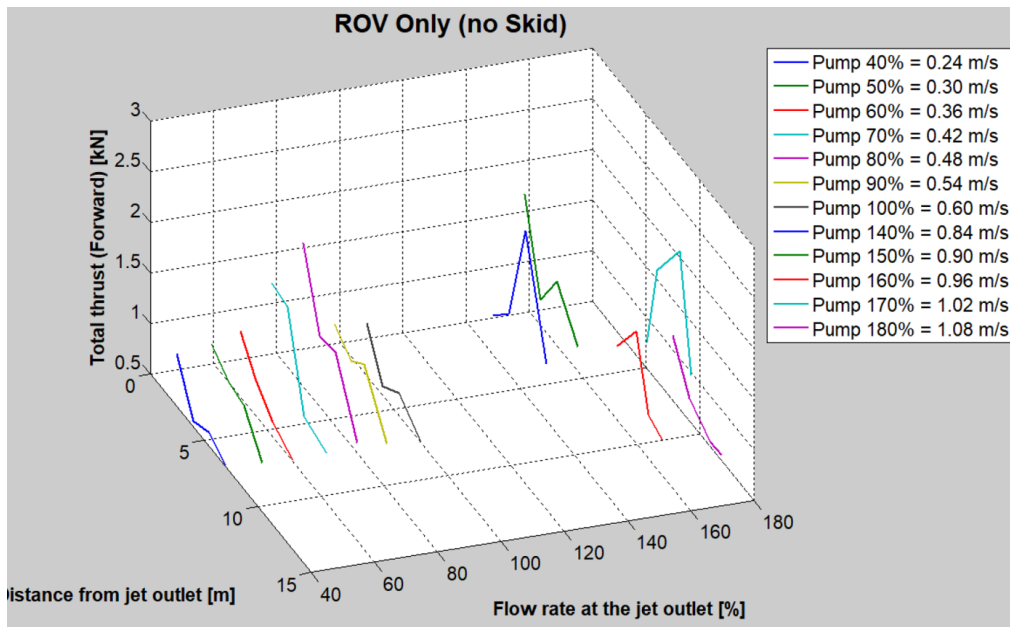


Figure 76: Total forward thrust vs distance from jet outlet and flow rate.

From the plot, some consistency is observed on water flow rates up to the full capacity of one pump (100% pump capacity representing ~ 0.6 m/s). ROV maneuverability for holding station off the bottom tank and along the jet axis was achievable, as illustrated in Figure 77 below.

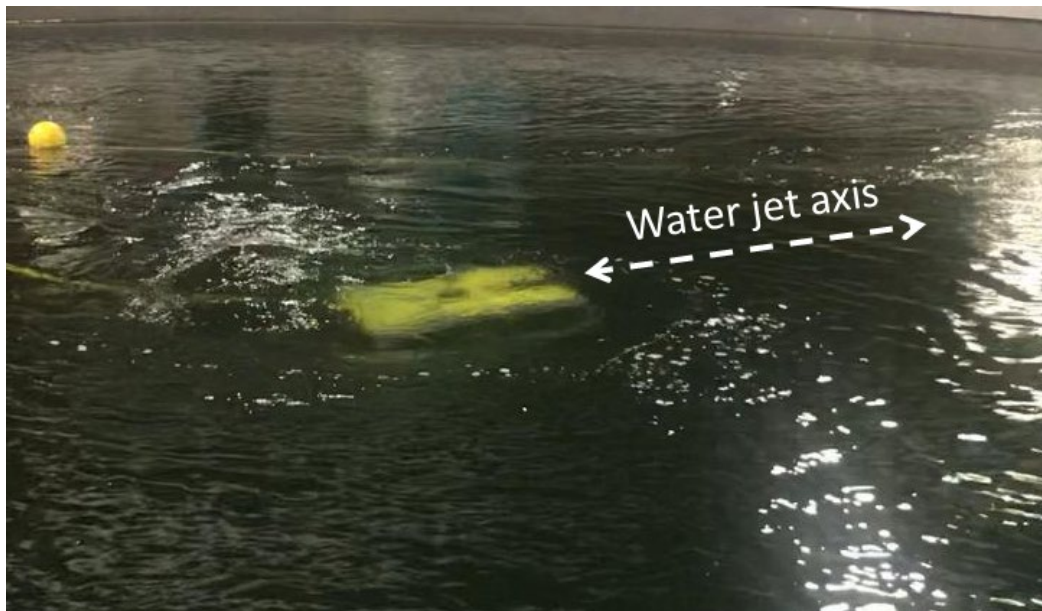


Figure 77: ROV holding station off the bottom tank, along the water jet axis.

Figure 78 below shows a zoom-out of the previous plot with high discrepancies in the data, illustrating the impossibility to control the maneuverability of the ROV for flow rates above 0.6 m/s. The plot is displayed with data table values for 140 and 150% pump capacities, highlighting the total forward thrust at 2.5 m away from the water jet outlet (dotted line arrows).

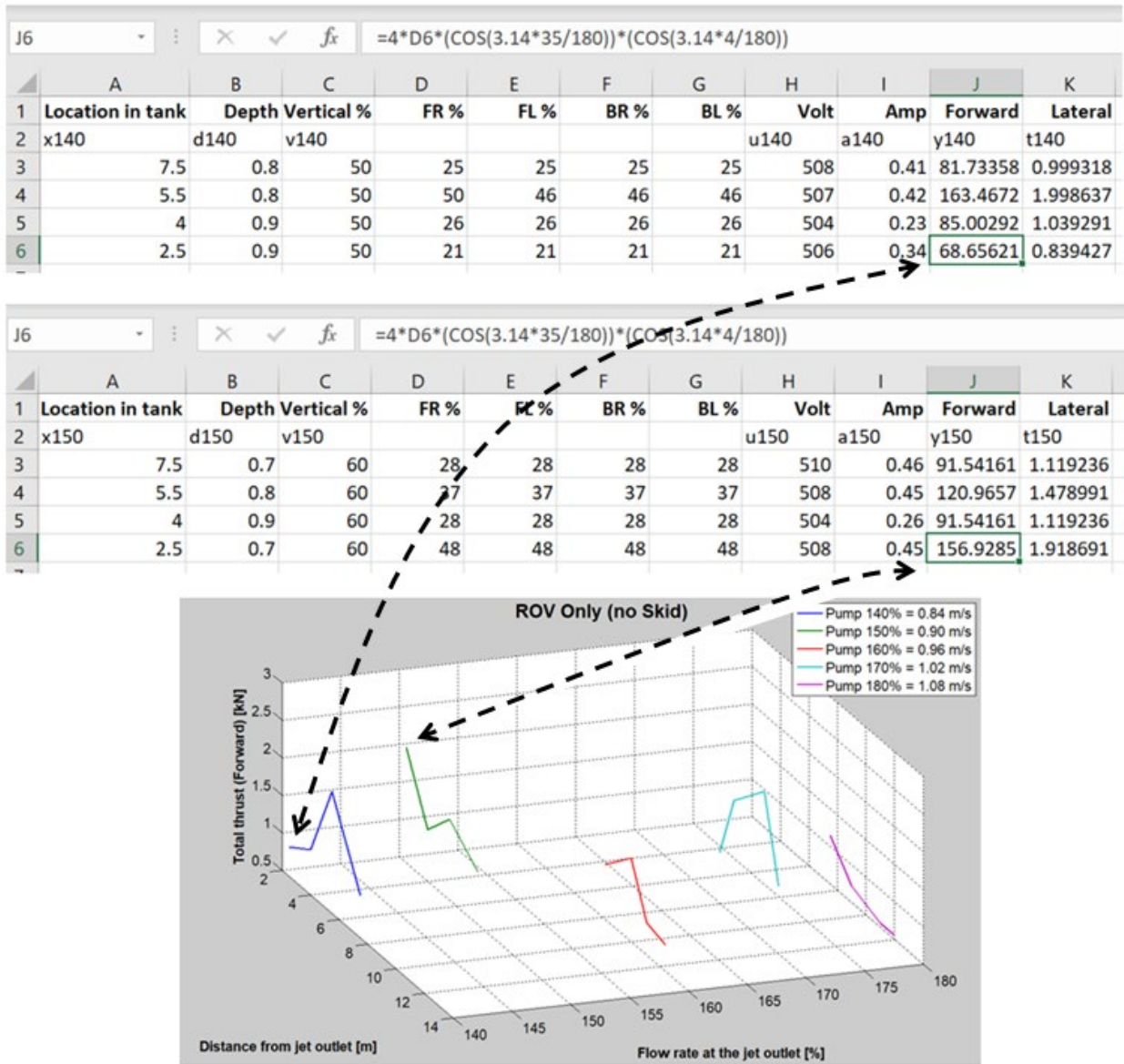


Figure 78: Zoom-out of the previous plot with high discrepancies in the data, illustrating the impossibility to control the maneuverability of the ROV for flow rates above 0.6 m/s.

Figure 79 below shows a 3D mesh of data points in space as well as a 3D surface plot of the data. This representation is useful for visualizing matrices that are too large to display in numerical form and for graphing functions of two variables. This therefore forms the baseline for future work on improving the proposed modeling capabilities, when collecting enough data to refine the results is possible.

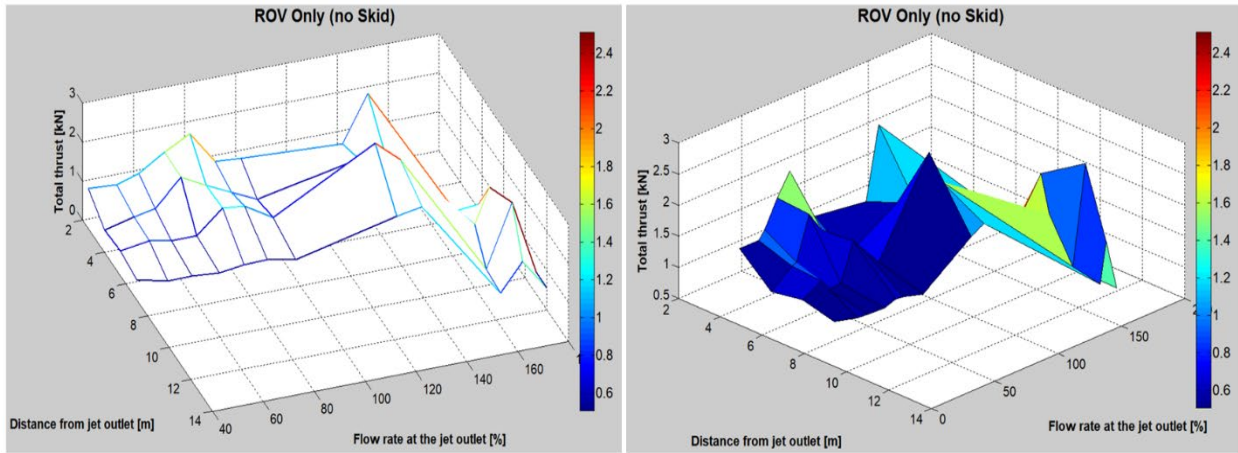


Figure 79: 3D mesh of data points in space (left) and 3D surface plot of the data (right).

Figure 80 below shows the correlation between the simulated Forward Total Thrust at the water jet outlet and the experimental values at 7, 5, 4 and 3m away from the jet outlet. Once again, an acceptable agreement is observed for flow rates up to 100% of one pump’s full capacity.

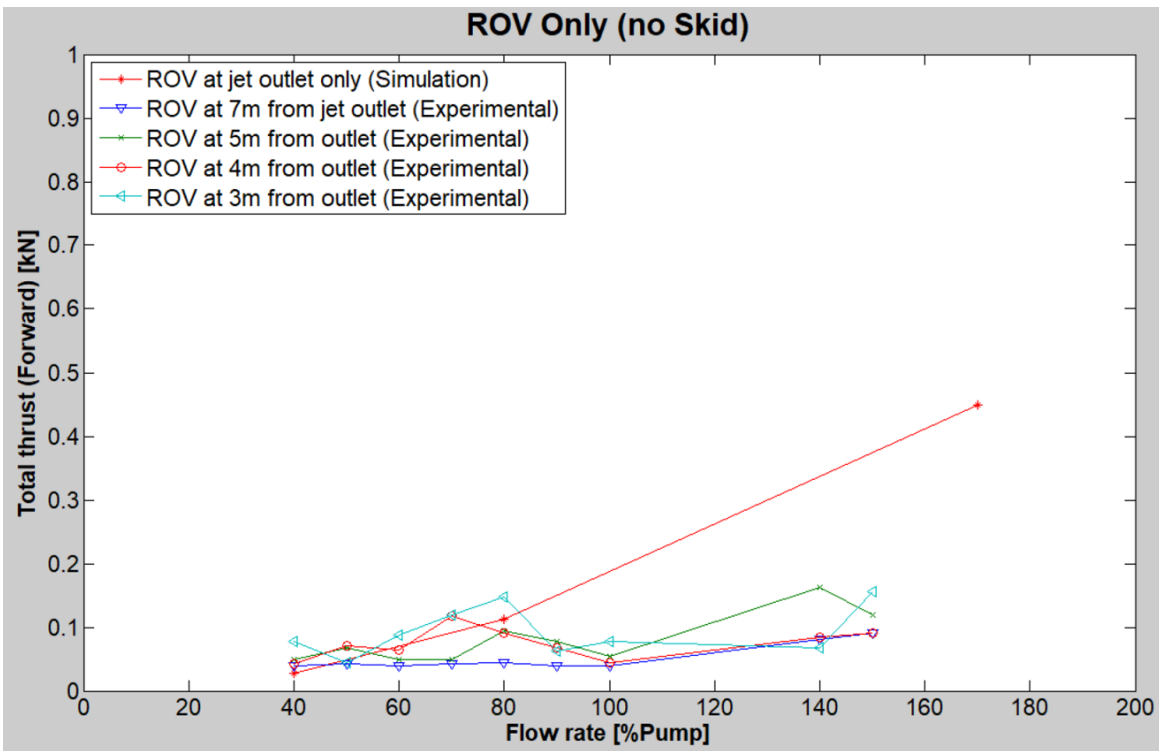


Figure 80: Forward Total Thrust simulation vs experiment.

Because the Aquatron facility was not operating at its full (four pumps) capacity (two pumps were not functioning), we have not been able to collect consistent data as more flow (power) was required due to increased inertia in the ROV. However, the few data collected are being processed and will be presented at an OERA webinar scheduled on December 12, 2019.

IX- CONCLUSIONS

The following conclusions can be drawn:

- Baseline capabilities of the Cougar ROV were established in Work Package 1. These capabilities can enable defining suitable operational windows appropriate for using ROVs with similar characteristics in marine operations in the Bay of Fundy. The results also adds to the body of knowledge available to DDL on their ROV type.
- The baseline capabilities established in Work Package 1 have enabled the improvement of available modeling capabilities in Work Package 2. The research has developed a method for applying a heuristic and evolutionary algorithms approach to optimizing data processing in the ProteusDS software. This results in a better data handling and reduction in computational time, giving the basis for development of robust ROV controllers. The proposed simulation-based optimization uses Surrogate Modeling (SM), Machine Learning (ML), and Efficient Global Optimization (EGO), and the knowledge has been transferred to DSA through discussions during the course of the project. A specific report on the practice is being prepared and will be shared with DSA by the end of January 2020, along with the NSERC Engage report.
- The project has demonstrated the feasibility of using ShipMo3D and NEMOH for the determination of added mass at infinite frequency, rather than the commonly used WAMIT, which is the most advanced set of tools available for analyzing wave interactions with offshore platforms and other structures or vessels. This has benefit to other SMEs in the sector, not able to afford expensive tools required to conduct their activities.
- Testing at the Aquatron Facility at Dalhousie University has enabled to measure and record the reaction loads of the Falcon ROV at different configurations in a controlled flow environment. The values are compared with the predictions obtained from ProdeusDS modeling software. We observe a good agreement between the experiments and the model for the ROV with no skid, at flow rates up to 100% of one pump's full capacity (corresponding to ~0.6 m/s). However, several discrepancies appear between the experiments and the model at higher flow rates above 140% (corresponding to ~0.84 m/s), illustrating a challenging or impossible maneuverability of the Falcon ROV. This information may improve marine operations in the Bay of Fundy by enabling a proper selection of intervention tasks and operational window for ROV deployment.

The main challenges encountered during the course of this project were:

- The unavailability of the Cougar ROV and introduction of the Falcon ROV to the study only two weeks before tank testing and 3 weeks before project closure, forcing the research team to generate (computationally demanding) new simulation data in an extremely short time-period.

- The lack of (cash/in-kind) leverage funding that has led to multiple scope revisions and cancellation of the Bay of Fundy field trials.
- The long waiting time as a result of legal teams reviewing updated agreement due to scope modifications.

X- RECOMMENDATIONS

Despite these positive observations, there are still many technical challenges to be tackled in developing optimum modeling capabilities for ROV maneuverability in high flow environments. These challenges are critical to industry advance, and thereby pose an opportunity for innovation, such as in control systems and software that increase yield to improve the way an ROV interacts in high flow environments such as adjusting pitch, yaw, height and others. Although the experiments performed provide a general understanding about the main difficulties encountered during ROV operations, the model has limitations in creating the actual environment and boundary conditions in the Aquatron Pool Tank. A dedicated study of this issue is needed and will further enable the improvement of modeling capabilities for ROV simulation. Moreover, testing in a more realistic environment where the umbilical's effect is not neglected is paramount. This will enable validation of the Euler-Bernoulli beam equations proposed. The proposed model could be used for simulating both the rigid body forces and the hydrodynamic forces, and may easily be extended to include additional effects such as non-neutral buoyancy and surface ship motions. This would then provide a better platform for modeling umbilical dynamics and its effect on ROV performance.

On a more practical standpoint, NSCC is involved in ocean floor mapping research in the Bay of Fundy. In this sector, sustainable management of marine resources requires spatial information, often in the form of maps. Developments in the field of acoustic remote sensing such as multibeam echo-sounders (MBES) combined with in situ sampling (i.e. video, stills, and grab samples) have allowed for the development of high-resolution seafloor maps, however not yet in high flow tidal environments such as in the Bay of Fundy. These maps can dramatically improve our understanding of the spatial patterns and complexities of the benthic environment. In practice, the imagery data can be collected using an ultra-high definition underwater drop video system. The camera system is lowered from a vessel, and drifts ~1m above the seafloor at pre-selected survey stations recording georeferenced footage of seafloor sediments and biota. Information from the video can then be spatially interpreted using the MBES data to generate the maps. However, strong tidal currents in certain parts of the Bay of Fundy make operation of the drop camera system challenging. In such locations, the use of a ROV platform as a long-term target of this DEMO project would be highly desirable. This will enable an improved MBES data ground-truthing, with the goal of generating a series of benthic habitat maps for the bay to facilitate fisheries management, and for use by the fishing industry to target fishing activities. NSCC will be looking for another industry partner to explore this research opportunity.

The information from this applied research project will definitely support overcoming the hurdles in improving modeling capabilities for marine operations in high flow environments. The skills gained will be transferable to other industry partners in need through joint initiatives, as effective software development can evolve to a financial force that can greatly improve the competitive environment within the private sector. OERA has also scheduled a webinar on December 12, 2019, for sharing the outcome of this project with the community. The research team is also preparing

two to three journal publications out of this work, among which one will be a dataset to an appropriate public data repository.

XI- BUDGET

Document forwarded separately.

XII- EMPLOYMENT SUMMARY

Table 4 below summarizes the names, positions and roles of the students and staff that participated on the project.

Table 4: Employment summary.

Name	Position	Role
Smith, Nick	Student	Mechanical design
Walsh, Corwin Douglas	Student	Electro-mechanical integration
Landry, Francois Joseph	Student	ROV electronic components assessment
Sherkat, Aliakbar	Student	Mechanical design
Kamga, Jordan Sop Fozin	Student	Hydrodynamics modeling
MacDonald, Neil	Research Assistant	Mechanical design and 3D modeling
MacNaughton, Thomas	Research Assistant	Mechanical design and 3D modeling
Abumousa, Shaza	Research Assistant	Analytical modeling
Osbourne, Nicholas	Research Associate	Hydrodynamics modeling
Shamma, Mo	Research Associate	ROV & umbilical modeling, project scope modification, data consolidation/analysis
Boachie, Ruth Takywaah	Research Associate	Explore applications for NSERC proposal
Sakib, Khan Ismam	Research Associate	Mechanical design and 3D modeling
Tsao, Jack	Research Associate	Applications for benthic habitat maps